

















ORIGINAL ARTICLE

Special Issue: The Brain in Flux: Genetic, Physiologic, and Therapeutic Perspectives on Transporters in the Nervous System

Bioisosteric analogs of MDMA: Improving the pharmacological profile?

Ana Sofia Alberto-Silva¹  | Selina Hemmer²  | Hailey A. Bock³  | Leticia Alves da Silva¹  | Kenneth R. Scott⁴  | Nina Kastner¹  | Manan Bhatt⁵  | Marco Niello¹  | Kathrin Jäntsch¹ | Oliver Kudlacek¹  | Elena Bossi^{5,6}  | Thomas Stockner¹  | Markus R. Meyer²  | John D. McCorvy^{3,7,8}  | Simon D. Brandt⁹  | Pierce Kavanagh⁴  | Harald H. Sitte^{1,10,11} 

¹Center for Physiology and Pharmacology, Institute of Pharmacology, Medical University of Vienna, Vienna, Austria

²Department of Experimental and Clinical Toxicology, Institute of Experimental and Clinical Pharmacology and Toxicology, Center for Molecular Signaling (PZMS), Saarland University, Homburg, Germany

³Department of Cell Biology, Neurobiology and Anatomy, Medical College of Wisconsin, Milwaukee, Wisconsin, USA

⁴Department of Pharmacology and Therapeutics, School of Medicine, Trinity Centre for Health Sciences, St James Hospital, Dublin, Ireland

⁵Laboratory of Cellular and Molecular Physiology, Department of Biotechnology and Life Sciences, University of Insubria, Varese, Italy

⁶Center for Research in Neuroscience, University of Insubria, Varese, Italy

⁷Neuroscience Research Center, Medical College of Wisconsin, Milwaukee, Wisconsin, USA

⁸Cancer Center, Medical College of Wisconsin, Milwaukee, Wisconsin, USA

⁹School of Pharmacy and Biomolecular Sciences, Liverpool John Moores University, Liverpool, UK

¹⁰Hourani Center for Applied Scientific Research, Al-Ahliyya Amman University, Amman, Jordan

¹¹Center for Addiction Research and Science, Medical University of Vienna, Vienna, Austria

Correspondence

Harald H. Sitte, Center for Physiology and Pharmacology—Institute of Pharmacology, Medical University Vienna, Währinger Straße 13a, 1090 Vienna, Austria.
Email: harald.sitte@meduniwien.ac.at

Present address

Marco Niello, Genetics of Cognition Laboratory, Istituto Italiano di Tecnologia, Genoa, Italy
Kathrin Jäntsch, Institute of Hygiene, Microbiology and Environmental Medicine, Department of Bacteriology, Medical University of Graz, Graz, Austria.

Abstract

3,4-Methylenedioxymethamphetamine (MDMA, 'ecstasy') is re-emerging in clinical settings as a candidate for the treatment of specific neuropsychiatric disorders (e.g. post-traumatic stress disorder) in combination with psychotherapy. MDMA is a psychoactive drug, typically regarded as an empathogen or entactogen, which leads to transporter-mediated monoamine release. Despite its therapeutic potential, MDMA can induce dose-, individual-, and context-dependent untoward effects outside safe settings. In this study, we investigated whether three new methylenedioxy bioisosteres of MDMA improve its off-target profile. In vitro methods included radiotracer

Abbreviations: BRET, bioluminescence resonance energy transfer; CL_{int} , intrinsic clearance; $CL_{int,micr}$, microsomal intrinsic clearance; CYP, cytochrome P450; DA, dopamine; DAT, dopamine transporter; DDIs, drug–drug interactions; DFIs, drug–food interactions; EC_{50} , half-maximal effective concentration; E_{MAX} , maximum effect; FMO3, flavin-containing monooxygenase 3; HEK293 cells, human embryonic kidney 293 cells; IC_{50} , half-maximal inhibitory concentration; LC-HRMS, liquid chromatography–high resolution mass spectrometry; MDA, 3,4-methylenedioxyamphetamine; MDMA, 3,4-methylenedioxyamphetamine; MPP⁺, 1-methyl-4-phenylpyridinium; MS, mass spectrometry; NE, norepinephrine; NET, norepinephrine transporter; OCT, organic cation transporter; ODMA, 1-(2,1,3-benzoxadiazol-5-yl)-N-methylpropan-2-amine; pCA, para-chloroamphetamine; pHLC, pooled human liver cytosol; pHLM, pooled human liver microsomes; PMAT, plasma membrane monoamine transporter; pS9, pooled human liver S9 fraction; PTSD, post-traumatic stress disorder; SeDMA, 1-(2,1,3-benzoselenadiazol-5-yl)-N-methylpropan-2-amine; SERT, serotonin transporter; SSRI, selective serotonin reuptake inhibitor; $t_{1/2}$, in vitro half-life; TDMA, 1-(2,1,3-benzothiadiazol-5-yl)-N-methylpropan-2-amine; 5-HT, 5-hydroxytryptamine; serotonin.

This is an open access article under the terms of the [Creative Commons Attribution](https://creativecommons.org/licenses/by/4.0/) License, which permits use, distribution and reproduction in any medium, provided the original work is properly cited.

© 2024 The Author(s). *Journal of Neurochemistry* published by John Wiley & Sons Ltd on behalf of International Society for Neurochemistry.

Funding information

National Institutes of Health, Grant/Award Number: R01 MH133849; Horizon 2020 Framework Programme, Grant/Award Number: 860954; Austrian Science Fund, Grant/Award Number: P32017, P35589 and W1232

assays, transporter electrophysiology, bioluminescence resonance energy transfer and fluorescence-based assays, pooled human liver microsome/S9 fraction incubations, metabolic stability studies, isozyme mapping, and liquid chromatography coupled to high-resolution mass spectrometry. In silico methods included molecular docking. Compared with MDMA, all three MDMA bioisosteres (ODMA, TDMA, and SeDMA) showed similar pharmacological activity at human serotonin, dopamine, and norepinephrine transporters (hSERT, hDAT, and hNET, respectively) but decreased agonist activity at 5-HT_{2A/2B/2C} receptors. Regarding their hepatic metabolism, they differed from MDMA, with *N*-demethylation being the only metabolic route shared, and without forming phase II metabolites. In addition, TDMA showed an enhanced intrinsic clearance in comparison to its congeners. Additional screening for their interaction with human organic cation transporters (hOCTs) and plasma membrane monoamine transporter (hPMAT) revealed a weaker interaction of the MDMA analogs with hOCT1, hOCT2, and hPMAT. Our findings suggest that these new MDMA bioisosteres might constitute appealing therapeutic alternatives to MDMA, sparing the primary pharmacological activity at hSERT, hDAT, and hNET, but displaying a reduced activity at 5-HT_{2A/2B/2C} receptors and alternative hepatic metabolism. Whether these MDMA bioisosteres may pose lower risk alternatives to the clinically re-emerging MDMA warrants further studies.

1 | INTRODUCTION

3,4-Methylenedioxymethamphetamine (MDMA, also known as 'ecstasy'; Figure 1a) is a psychoactive drug capable of inducing a "controlled altered state of consciousness" (Shulgin & Nichols, 1978). In recent years, MDMA re-emerged in preclinical and clinical research for the treatment of specific neuropsychiatric disorders, such as post-traumatic stress disorder (PTSD), in combination with psychotherapy (Mitchell et al., 2021, 2023; Mithoefer et al., 2011, 2018).

MDMA is a ring-substituted amphetamine derivative with psychostimulant activity. MDMA is unique in inducing an interoceptive and prosocial effect, and it has been described as an empathogen or entactogen (Nichols, 1986). Although its mechanism of action is not yet fully elucidated, MDMA is generally recognized to interact with monoamine transporters for serotonin (SERT), dopamine (DAT), and norepinephrine (NET), eliciting non-exocytotic efflux of serotonin (5-hydroxytryptamine; 5-HT), dopamine (DA) and norepinephrine (NE), respectively (Rothman et al., 2001; Rudnick & Wall, 1992). Additionally, MDMA is an agonist at 5-HT_{2A/2B/2C} receptors (Nash et al., 1994; Setola et al., 2003). The reported acute and chronic side effects of MDMA can range from tachycardia and hypertension to hyperthermia, cardiotoxicity, and hepatotoxicity (Bhattacharyya et al., 2009; Capela, Meisel, et al., 2006a; Capela, Ruscher, et al., 2006b; Delaforge et al., 1999; Dunlap et al., 2018; Fonseca et al., 2021; La Torre et al., 2004; Setola et al., 2003; Steinkellner et al., 2011; Vizeli et al., 2017; Vollenweider et al., 1998).

MDMA is rapidly absorbed in the intestinal tract and its metabolism displays non-linear pharmacokinetics, which has been partially linked to the inhibition of certain cytochrome P450 (CYP) enzymes (Dunlap et al., 2018; La Torre et al., 2004; Yang et al., 2006). This enzymatic inhibition has mainly been associated with the methylenedioxy group of MDMA (Delaforge et al., 1999; Dinger et al., 2016; La Torre et al., 2004). Additionally, the metabolites of MDMA have been described to be responsible for MDMA-related neurotoxicity in rodents, since bypassing metabolism through direct intracerebroventricular administration of MDMA did not induce neurotoxicity in these studies (Esteban et al., 2001; Green et al., 2003; Paris & Cunningham, 1992). Moreover, it was reported that MDMA metabolites (mainly catechol and quinone metabolites formed after opening of the methylenedioxy group) could generate free radicals (e.g. reactive oxygen species), which might induce oxidative stress and cellular damage (Capela, Meisel, et al., 2006a; Jayanthi et al., 1999; Shankaran et al., 1999).

In this study, we investigated three new MDMA analogs with a bioisosteric replacement of the methylenedioxyphenyl (or 1,3-benzodioxole) group of MDMA. This chemical modification has been described to be able to evade the inhibition of CYP enzymes, namely CYP2D6 (Anzali et al., 1997; Meanwell, 2014). The analogs were designed by the replacement of the 1,3-benzodioxole group with 2,1,3-benzoxadiazole, 2,1,3-benzothiadiazole, and 2,1,3-benzoselenadiazole, which gave 1-(2,1,3-benzoxadiazol-5-yl)-*N*-methylpropan-2-amine (ODMA), 1-(2,1,3-benzothiadiazol-5-yl)-*N*-methylpropan-2-amine (TDMA), and 1-(2,1,3-benzoselenadiazol

-5-yl)-*N*-methylpropan-2-amine (SeDMA), respectively (Figure 1a). The main aims of this study were to characterize the molecular mode of action of these three analogs at key targets: monoamine transporters (SERT, DAT, and NET), a subset of serotonin receptors (subfamily 2), organic cation transporters, and plasma membrane monoamine transporters. In addition, we studied the *in vitro* hepatic metabolism of these MDMA analogs and how it differed from MDMA. Considering the reported MDMA-induced adverse events, it is advantageous to explore MDMA-related congeners which can putatively keep or improve its therapeutic action but potentially decrease its off-target effects.

2 | MATERIALS AND METHODS

See the Supplementary Information (SI) for the complete details in each section.

2.1 | Drugs and reagents

The experimental drug MDMA hydrochloride (HCl; MW=229.7 g/mol) was purchased from Lipomed AG (Arllesheim, Switzerland; cat. no. MDM-94-HC) or Cayman Chemical (Ann Arbor, MI, USA; cat. no. 13971). ODMA HCl (MW=227.69 g/mol), TDMA HCl (MW=243.75 g/mol) and SeDMA succinate (MW=254.19:118.09 g/mol; ≥95%) were synthesized using established methods (Abdel-Magid et al., 1996; Briner et al., 2000; Gadakh et al., 2014). Identity and purities were confirmed by standard analytical characterizations. All MDMA and analogs were racemates (\pm ; *R/S*). Other experimental drugs comprised vanoxerine (GBR12909; cat. no. D052), *para*-chloroamphetamine (*p*CA) HCl (cat. no. C9635), dextroamphetamine hemisulfate salt (*d*-amp; (*S*)-amphetamine; cat. no. A5880), monensin (cat. no. M5273) and dopamine (DA; cat. no. H8502) which were supplied by Sigma-Aldrich (St. Louis, MO, United States). Serotonin (5-hydroxytryptamine; 5-HT) HCl (cat. no. 169300) was obtained from Fluorochem Ltd (Hadfield, United Kingdom) or from Sigma-Aldrich (cat. no. H7752), and paroxetine HCl (cat. no. AB 439408) was obtained from abcr GmbH (Karlsruhe, Germany). For cell culture, Dulbecco's Modified Eagle Medium (DMEM) high glucose (4.5 g/L) with L-glutamine (cat. no. DMEM-HA) and fetal bovine serum (FBS; cat. no. FBS-11A) were obtained from Capricorn Scientific GmbH (Ebsdorfergrund, Germany), as well as geneticin (G-418 sulfate solution; 50 mg/mL; cat. no. G418-B). Blasticidin (10 mg/mL; cat. no. ant-bl) and zeocin (100 mg/mL; cat. no. ant-zn) were purchased from InvivoGen (San Diego, CA, United States). Tetracycline HCl (cat. no. 84774020) was obtained from former Boehringer Mannheim (Mannheim, Germany). Penicillin-streptomycin (10000 IU/10 mg/100 mL; cat. no. P4333) was purchased from Sigma-Aldrich (St. Louis, MO, United States). For radiolabeled assays, [³H]5-HT (1 mCi; cat. no. NET498) and [³H]1-methyl-4-phenylpyridinium ([³H]MPP⁺; 250 μ Ci; cat. no. NET914) were obtained from Revvity (former PerkinElmer, Inc; Waltham, MA, USA).

See the Supporting Information for complete details on the chemical synthesis of the experimental compounds ODMA, TDMA, and SeMA, and other drugs and reagents.

2.2 | Cell culture

Human embryonic kidney 293 (HEK293) cells stably expressing the human isoforms (h) of SERT, DAT, NET, OCT1-3, and PMAT were used. HEK293 cells are not listed by the International Cell Line Authentication Committee (ICLAC, <https://iclac.org/databases/cross-contaminations/>) as commonly misidentified cell line. The HEK293 cells were last authenticated on 11-Apr-2024 by the Medical University Vienna, Austria. Except for hNET, YFP-tagged constructs were used in uptake-inhibition and release assays. The generation and maintenance of stable cell lines expressing hSERT, hDAT or hNET were conducted as previously described (Mayer et al., 2016). For hOCTs and hPMAT, their generation and maintenance followed similar procedures (Maier, Rauter, et al., 2021b). The cell lines were maintained in high glucose (4.5 g/L) and L-glutamine-containing DMEM, supplemented with 10% FBS, 1 μ g/mL streptomycin, 100 IU/mL penicillin, and G418 (250 μ g/mL) in a humidified atmosphere (37°C, 5% CO₂) and a subconfluent state. The cells were typically not passaged over 25 times. For 5-HT₂ G protein dissociation assays, HEK 293T cells (ATCC; RRID:CVCL_0063) were used and tested to be mycoplasma-free. For 5-HT₂ Gq-mediated calcium flux assays, stably-expressing 5-HT_{2A/2B/2C} receptor Flp-In 293T-Rex cells (RRID:CVCL_U427) were used and tested to be mycoplasma-free.

2.3 | Uptake inhibition and release assays

Experiments were conducted in HEK293 cells as previously described (Mayer et al., 2016; Nadal-Gratacós et al., 2021), with minor modifications. Radiotracers were [³H]5-HT for hSERT and [³H]MPP⁺ for hDAT, hNET, hOCT1-3, and hPMAT. In uptake inhibition assays, non-specific uptake was determined in the presence of paroxetine (3 μ M) for hSERT, GBR12909 (50 μ M) for hDAT and hNET, and decynium-22 (D22; 100 μ M) for hOCT1-3 and hPMAT, and represented <10% of total uptake. Uptake-inhibition curves were plotted and fitted by non-linear regression, and data were best fitted to a sigmoidal dose-response curve to obtain IC₅₀ values from at least three independent cell culture preparations ($n \geq 3$), performed in triplicate. 1/hDAT IC₅₀:1/hSERT IC₅₀ formula was used to calculate hDAT/hSERT ratios. In release assays, to determine the specificity of drug-induced reverse transport, selective transporter inhibitors and effective releasers were used, respectively: paroxetine (0.05 μ M) and *p*CA (10 μ M) for hSERT, GBR12909 (0.5 μ M) and (*S*)-amphetamine (10 μ M) for hDAT, and nisoxetine (30 μ M) and (*S*)-amphetamine (10 μ M) for hNET. Data are mean \pm SD from three to five independent cell culture preparations ($n=3-5$), performed in duplicate (batch release assays (hSERT)) or triplicate (superfusion release assays (hDAT and

hNET)). The efflux elicited by two different conditions ((1) compound in vehicle (Krebs-HEPES buffer (KHB)) or (2) compound in monensin (10 μ M; MON)) was compared at the indicated time points. See the Supporting Information for complete details.

2.4 | Transporter electrophysiology: HEK293 cells and *Xenopus laevis* oocytes

HEK293 cells overexpressing the transporter of interest were used. For hDAT, a stably expressing cell line was used (Giros et al., 1992; Sitte et al., 1998). For hSERT, a cell line with a GFP-tagged version of the transporter in a tetracycline-inducible construct was used as previously described (Hasenhuettl et al., 2018). *Xenopus laevis* oocytes were injected with in vitro transcribed cRNA of either hDAT or hSERT. Subsequent electrophysiological studies were performed using the two-electrode voltage clamp technique (Oocyte Clamp OC-725; Warner Instruments, Hamden, CT, USA; Bhatt et al., 2022; Vacca et al., 2022). The animal study was reviewed and approved by the Committee of the "Organismo Preposto al Benessere degli Animali" of the University of Insubria and nationally by Ministero della Salute (permit no. 449/2021-PR). The portions of the ovary were used according to the Italian Law Art. 18 (3'R) 316 DLgs26_2014. See the Supporting Information for complete details.

2.5 | Gq dissociation bioluminescence resonance energy transfer (BRET): 5-HT_{2A/2B/2C} receptor activity

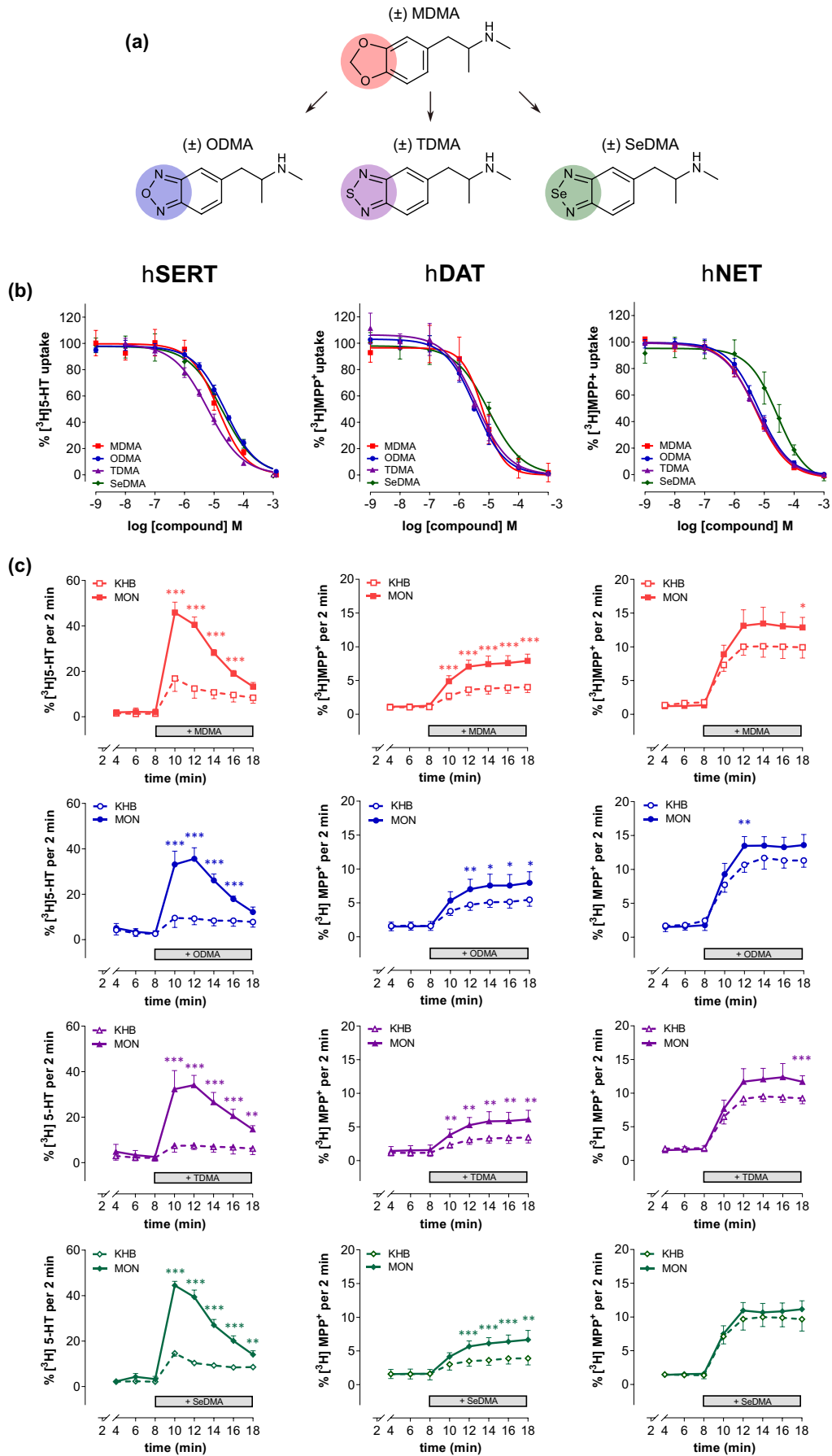
5-HT₂ Gq dissociation BRET assays were performed as previously described (Cunningham et al., 2023; Lewis et al., 2023). HEK 293T cells (ATCC) were transfected in 10% dialyzed FBS (dFBS; Omega

Scientific) in a 1:1:1:1 ratio of human receptor:Gαq-Rluc8:β3:GFP2-γ9 DNA constructs prepared in Opti-MEM (Invitrogen) using a 3:1 ratio of TransIT-2020 (Mirus Bio) μ L:μg total DNA. Next day, cells were detached, centrifuged, resuspended and plated in 1% dFBS at an approximate density of 30000 cells per well into poly-L-lysine-coated 96-well white assay plates (Greiner Bio-One). After approximately 24 h, media was decanted and replaced with 60 μ L per well of drug buffer (1× HBSS, 20 mM HEPES, pH 7.4), and incubated for at least 15 min at 37°C in a humidified incubator before receiving drug stimulation. Drug dilutions were made in drug buffer containing 0.3% BSA fatty acid free and 0.03% ascorbic acid. Drug dilutions were dispensed in 30 μ L per well using multi-channels and plates were incubated at 37°C in a humidified incubator until reading. Next, plates were briefly taken out and coelenterazine 400a (5 μ M final concentration; Nanolight Technology) was added 15 min before reading. After 60 min total time of drug incubation, plates were read in a PheraStarFSX or ClarioStar Plus (BMG Labtech; Cary, NC) at 1 s per well for at least 15 min for 3–5 cycles. BRET ratios of 510/400 luminescence were calculated per well and were plotted as a function of drug concentration. Data were normalized to % positive control (5-HT) stimulation and analyzed using nonlinear regression "log(agonist) vs. response" to yield E_{MAX} and EC_{50} parameter estimates. All assays were performed in duplicate with at least three independent cell culture preparations.

2.6 | FLIPR Gq-mediated calcium flux assays

Stably-expressing 5-HT_{2A/2B/2C} receptor Flp-In 293T-Rex Tetracycline inducible system (Invitrogen, mycoplasma-free) were used for calcium flux assays (Lewis et al., 2023). 5-HT_{2A/2B/2C} receptor constructs were derived from the codon-optimized Tango pcDNA3.1 library (Kroeze et al., 2015; Addgene) with V2tail/TEV/tTA encoding regions deleted to yield "de-Tango" constructs, and then shuttled into pcDNA5/

FIGURE 1 3,4-Methylenedioxymethamphetamine (MDMA) and its analogs 1-(2,1,3-benzoxadiazol-5-yl)-N-methylpropan-2-amine (ODMA), 1-(2,1,3-benzothiadiazol-5-yl)-N-methylpropan-2-amine (TDMA), and 1-(2,1,3-benzoselenadiazol-5-yl)-N-methylpropan-2-amine (SeDMA) interact at low micromolar concentrations with the monoamine transporters. (a) Chemical structures of (±) MDMA and its analogs (±) ODMA, (±) TDMA, and (±) SeDMA, in which the methylenedioxy group or its chemical modification is highlighted in red, blue, purple, or green, respectively. (b) Uptake inhibition curves at human serotonin transporter (hSERT) (left panel), human dopamine transporter (hDAT) (middle panel), and human norepinephrine transporter (hNET) (right panel). Data are mean \pm standard deviation (SD) from three to five independent cell culture preparations ($n=3-5$), performed in triplicate. Curves were plotted and fitted by non-linear regression, and data were best fitted to a sigmoidal dose–response curve to obtain half-maximal inhibitory concentration (IC_{50}) values (see Table 1). (c) Transporter-mediated release of preloaded [³H]substrate from human embryonic kidney 293 (HEK293) cells stably expressing hSERT, hDAT, or hNET. Compounds were added from 8 to 18 min at a concentration close to their IC_{50} value, either in vehicle (KHB) (empty symbols) or in monensin (10 μ M) (MON) (filled symbols); data are mean \pm SD from four to five independent cell culture preparations ($n=4-5$) performed in duplicate (batch release assays (hSERT) or in triplicate (superfusion release assays (hDAT and hNET))). A statistical analysis with a mixed-effects model employing Šidák correction for multiple comparisons confirmed significant differences between KHB and MON conditions at the indicated time points, thus validating the releasing capabilities of the compounds. For control experiments with known full releasing agents or inhibitors at each transporter, see Figure S1. Statistical significance was defined at a p value less than 0.05. *denotes $p < 0.05$, ** $p < 0.01$, and *** $p < 0.001$ (from left to right: p values for hSERT–MDMA: $p \leq 0.0001$, < 0.0001 , < 0.0001 , 0.0007 , respectively, $df = 13-17$; ODMA: $p \leq 0.0001$ (all), $df = 13-17$; TDMA: $p = 0.001$, < 0.0001 , < 0.0001 , 0.0001 , 0.0037 , $df = 11-14$; SeDMA: $p \leq 0.0001$, < 0.0001 , < 0.0001 , 0.0006 , 0.0048 , $df = 7-12$; p values for hDAT–MDMA: $p \leq 0.0001$ (all), $df = 19-22$; ODMA: $p = 0.0067$, 0.0104 , 0.0132 , 0.0139 , $df = 17-19$; TDMA: $p = 0.0044$, 0.0015 , 0.0035 , 0.0011 , 0.0063 , $df = 14-19$; SeDMA: $p \leq 0.0001$, < 0.0001 , < 0.0001 , 0.0038 , $df = 18-22$; p values for hNET–MDMA: $p = 0.0312$, $df = 18$; ODMA: $p = 0.0013$, $df = 21$; TDMA: $p = 0.0005$, $df = 16$). Full statistical reports can be found in the SI.



	$[^3\text{H}]5\text{-HT}$ uptake, IC_{50} (μM) hSERT	$[^3\text{H}]MPP^+$ uptake, IC_{50} (μM) hDAT	$[^3\text{H}]MPP^+$ uptake, IC_{50} (μM) hNET	hDAT/hSERT ratio
(\pm) MDMA	13.7 \pm 1.6	6.2 \pm 2.6	4.9 \pm 0.3	2.20
(\pm) ODMA	23.9 \pm 5.0	4.0 \pm 1.5	6.6 \pm 1.6	5.97
(\pm) TDMA	6.4 \pm 1.0	4.5 \pm 1.3	5.6 \pm 1.8	1.41
(\pm) SeDMA	19.1 \pm 4.2	9.8 \pm 2.2	22.1 \pm 8.6	1.95

Note: The potency of MDMA and its analogs ODMA, TDMA, and SeDMA at hSERT, hDAT, and hNET. Data represent mean and SD from at least three independent cell culture preparations ($n \geq 3$) performed in triplicate. DAT/SERT ratio = $(1/\text{DAT}_{\text{IC}_{50}}):(1/\text{SERT}_{\text{IC}_{50}})$.

FRT/TO using Gibson Assembly. Cell lines were maintained in high-glucose DMEM (VWR) containing 10% FBS (Life Technologies), 10 $\mu\text{g}/\text{mL}$ Blasticidin (GoldBio), and 100 $\mu\text{g}/\text{mL}$ Hygromycin B (GoldBio). Approximately 1 day before the assay, tetracycline (2 $\mu\text{g}/\text{mL}$) was used to induce receptor expression and approximately 7500 cells per well in DMEM containing 1% dialyzed FBS were seeded into 384-well poly-L-lysine-coated black plates. Next day, plate media was decanted, and Fluo-4 Direct dye reconstituted in drug buffer (1 \times HBSS, 20 mM HEPES, pH 7.4) containing 2.5 mM probenecid was added (Invitrogen, 20 $\mu\text{L}/\text{well}$) and plates were incubated for approximately 60 min at 37°C. After dye load, plates were allowed to equilibrate to room temperature for 15 min, and then placed in a FLIPR^{TETRA} fluorescence imaging plate reader (Molecular Devices). Drug dilutions were prepared at 5X final concentration in McCorvy buffer (20 mM HEPES-buffered HBSS, pH 7.4 supplemented with 0.3% BSA fatty-acid free and 0.03% ascorbic acid). Drug dilutions were aliquoted into 384-well plastic plates and placed in the FLIPR^{TETRA} for drug stimulation. Fluorescence for the FLIPR^{TETRA} were programmed to read baseline fluorescence for 10 s (1 read/s), and afterward 5 μL of drug per well was added and read for a total of 2 min (1 read/s). Fluorescence in each well was normalized to the average of the first 10 reads for baseline fluorescence, and then both maximum-fold peak increase over basal and area under the curve (AUC) was calculated. Peak fold-over-basal was plotted as a function of drug concentration, and data were normalized to percent 5-HT stimulation. Data were plotted and non-linear regression was performed using "log(agonist) versus response" to yield E_{max} and EC_{50} parameter estimates. Data were normalized to % 5-HT response, where a full concentration-response 5-HT curve was present on every plate. All assays were performed in triplicate with at least three independent cell culture preparations.

2.7 | Calcium flux activity of 5-HT_{2A/2B/2C} receptors by GCaMP6s fluorescence

To further study the interaction of our test compounds with 5-HT_{2A}R and 5-HT_{2B}R, HEK293 cells were generated expressing tetracycline inducible CFP-tagged versions of 5-HT_{2A} and 5HT_{2B} receptor and a constitutively expressing Ca²⁺ sensor GCaMP6s (Chen et al., 2013), as previously described (Mayer et al., 2023). See the Supporting Information for complete details.

TABLE 1 Uptake inhibition assays.

2.8 | ELISA surface expression detection using FLAG-tag

Surface expression was measured by N-terminal FLAG-tagged ELISA detection. N-terminal FLAG-tagged 5-HT_{2A/2B/2C} receptor transfected HEK293 cells used in Gq dissociation BRET assays were plated in 1% dFBS at an approximate density of 30000 cells per well into poly-L-lysine-coated 96-well white assay plates (Greiner Bio-One). The next day, the media was decanted and 4% paraformaldehyde (PFA) in PBS was added to fix the cells for approximately 15–20 min. PFA was decanted and cells were washed with PBS. Then, 2% BSA PBS solution was added as a blocking solution for 30 min, followed by a 1/20000 diluted anti-FLAG HRP conjugated antibody (Sigma-Aldrich, cat. no. A8592) in 0.5% BSA PBS solution. Plates were incubated for 1 h at room temperature. Afterwards, cells were washed 3 \times with PBS, and then SuperSignal Pico Chemiluminescent Substrate was added to detect extracellular FLAG-tagged. Plates were then read for luminescence (LCPS) 15 min later on a Microbeta Trilux (PerkinElmer). Data were analyzed to calculate the average and SEM from three independent cell culture preparations and compared to a no-FLAG-tagged pcDNA3.1 empty vector control.

2.9 | Computational pharmacology

2.9.1 | Protein and ligand structures preparation

In this study, we utilized the hSERT structure (PDB ID: 5I71; (Coleman et al., 2016)). To generate homology models of hDAT based on the hSERT structure, we employed MODELER (Šali & Blundell, 1993). Prior to molecular docking, both proteins were submitted to molecular dynamics simulations following the established protocol described in previous studies (Gradisch et al., 2022; Szöllösi & Stockner, 2021). See the Supporting Information for complete details.

2.9.2 | Molecular docking

The ligands were docked into the protein with the co-transported ions bound using the GOLD (Genetic Optimization for Ligand

Docking) software version 2022.2.0 (Jones et al., 1997). See the Supporting Information for complete details.

2.10 | Hepatic metabolism

2.10.1 | Pooled human liver microsome/S9 fraction incubation for identification of phase I and II metabolites and isozyme mapping: LC-HRMS/MS conditions

Incubation using pooled human liver microsomes (pHLM) were prepared according to published procedures (Richter et al., 2016; Welter et al., 2013). ODMA, TDMA, or SeDMA were incubated with pooled human liver S9 fraction (pS9; 2 mg microsomal protein/mL) in accordance to a previous publication with minor modifications (Richter, Maurer, & Meyer, 2017b). Incubation conditions for isozyme mapping followed an established protocol (Wagmann et al., 2016).

Regarding LC-HRMS/MS conditions, and according to previously published procedures, analyses were performed using a Thermo Fisher Scientific (TF, Dreieich, Germany) Dionex UltiMate 3000 RS pump consisting of a degasser, a quaternary pump, and an UltiMate Autosampler, coupled with a TF Q Exactive Plus equipped with a heated electrospray ionization (HESI)-II source (Gampfer et al., 2019). See the Supporting Information for complete details.

2.10.2 | Metabolic stability studies

Metabolic stability studies were done by measuring substrate depletion of ODMA, TDMA, SeDMA, and MDMA according to Wagmann et al. (Wagmann et al., 2020). Briefly, incubations were performed using pHLM with the following modifications: 0.5 μ M substrate concentrations were used and incubations were stopped after 0, 15, 30, 60, 90, 120, and 150 min by addition of 50 μ L of ice-cold acetonitrile containing L-tryptophan- d_5 (5 mg/L). All incubations were performed in duplicate. Additionally, control incubations ($n=2$) without pHLM were prepared to observe enzyme independent degradation of parent compounds and stopped after 150 min. Mixtures were centrifuged at 18407g for 2 min. The resulting supernatants were transferred into LC vials and analyzed by LC-HRMS/MS. The degradation of parent compounds was further assessed by calculating the natural logarithm of the absolute peak area of the analyte in HR full scan.

2.11 | Statistical analysis

Data plotting and statistical analyses were performed with GraphPad Prism 5, 9 or 10 (GraphPad Software Inc., San Diego, CA, USA). Data are expressed as mean \pm standard error of mean (SEM) or mean \pm standard deviation (SD). Data were not assessed for normality and no tests for outliers were conducted. For both batch and

superfusion release assays, data were statistically analyzed using a mixed-effects model, employing Šidák's correction for multiple comparisons. This statistical analysis explored possible significant differences between KHB and MON conditions. Statistical significance was defined at a p -value less than 0.05. *denotes $p < 0.05$, ** $p < 0.01$ and *** $p < 0.001$. For metabolic stability studies, a t -test was conducted to determine if there were significant differences between $\ln[\text{peak area}]_{\text{initial}}$ values and $\ln[\text{peak area}]$ values in control incubations without pHLM, using the following settings: unpaired: two-tailed; significance level, 0.05; confidence intervals, 99%. Calculations were performed according to the equations of Baranczewski et al. (Baranczewski et al., 2006):

$$\ln[\text{peak area}]_{\text{remaining}} = \ln[\text{peak area}]_{\text{initial}} - k \times t \text{ and } t_{1/2} = \frac{\ln(2)}{k} \quad (1)$$

$$CL_{\text{int,micr}} = \frac{\ln(2)}{t_{1/2}(\text{min})} \times \frac{[V]_{\text{incubation}}(\text{mL})}{[P]_{\text{incubation}}(\text{mg})} \quad (2)$$

$$CL_{\text{int}} = CL_{\text{int,micr}} \left(\frac{\text{mL}}{\text{min} \times \text{mg}} \right) \times \frac{[\text{Liver}](\text{g})}{[\text{BW}](\text{kg})} \times SF \left(\frac{\text{mg}}{\text{g}} \right) \quad (3)$$

with k =slope of the linear regression fit, $t_{1/2}$ =in vitro half-life, $CL_{\text{intr,micr}}$ =microsomal intrinsic clearance, CL_{intr} =intrinsic clearance $[V]_{\text{incubation}}$ =incubation volume=0.05, $[P]_{\text{incubation}}$ =microsomal protein amount in incubation=0.05, $\frac{[\text{Liver}]}{[\text{BW}]}$ =liver weight normalized by body weight (Davies & Morris, 1993)=26, and SF =scaling factor microsomal protein per gram of liver (Baranczewski et al., 2006)=33.

3 | RESULTS

3.1 | MDMA and its analogs inhibit the [^3H] substrate uptake at hSERT, hDAT, and hNET at low micromolar concentrations in HEK293 cells

The interaction of MDMA (Figure 1a) with the monoamine transporters has been extensively investigated over the years (Baumann et al., 2012; Dolan et al., 2019; Kolaczynska et al., 2022; Luethi et al., 2019; Montgomery et al., 2007; Rudnick & Wall, 1992; Sandtner et al., 2016; Shimshoni et al., 2017). Thus, to start our molecular characterization, we first explored the capability of MDMA and its analogs to inhibit the substrate uptake at hSERT, hDAT, and hNET. The resulting uptake inhibition curves and the respective IC_{50} values were calculated (Figure 1b; Table 1) and it was found that MDMA and its analogs interacted with all monoamine transporters at low micromolar concentrations. Specifically, at hDAT and hNET, MDMA, ODMA, and TDMA had similar potencies inhibiting [^3H] MPP $^+$ uptake, resulting in virtually identical IC_{50} values, whereas SeDMA showed a slightly decreased inhibitory potency (hDAT: $IC_{50}=9.8 \pm 2.2 \mu\text{M}$; hNET: $IC_{50}=22.1 \pm 8.6 \mu\text{M}$), being about half or a quarter less potent than its congeners, respectively. At hSERT, TDMA was 2-fold more potent ($IC_{50}=6.4 \pm 1.0 \mu\text{M}$) than MDMA in

inhibiting [^3H]5-HT uptake, whereas ODMA was 2-fold less potent. In contrast, SeDMA displayed a similar inhibitory potency compared with MDMA. Due to each compound similar uptake inhibitory potencies at hSERT and hDAT, the calculated hDAT/hSERT ratios (Table 1) resulted in low values (<10), suggesting a low abuse liability for these compounds (Baumann et al., 2011; Luethi & Liechti, 2020; Simmler et al., 2013).

3.2 | MDMA and its analogs evoke robust [^3H] substrate release at hSERT and hNET, but moderate at hDAT

In order to establish the substrate vs. inhibitor profile of each experimental drug at hSERT, hDAT, and hNET, the calculated IC_{50} values from the previous uptake inhibition assays were used in the subsequent release assays in HEK293 cells. In these experiments, the time-dependent efflux of [^3H]5-HT through hSERT and of [^3H]MPP $^+$ through hDAT or hNET was evaluated in the presence or absence of monensin (10 μM). Monensin is an ionophore that dissipates the sodium gradient across cell membranes that selectively enhances the efflux caused by transporter substrates, which helps to distinguish them from non-transported inhibitors (Scholze et al., 2000). At hSERT, MDMA and the three test drugs elicited a significant release of [^3H]5-HT in the presence of monensin (Figure 1c, left panels), when compared with negative and positive controls (paroxetine (0.05 μM) and *para*-chloroamphetamine (*p*CA; 10 μM), respectively; Figure S1). On the other hand, at hDAT, MDMA and its analogs evoked a moderate release of [^3H]MPP $^+$ over time in the presence of monensin (Figure 1c, middle panels), compared with the negative and positive controls (GBR12909 (0.5 μM) and (*S*)-amphetamine (10 μM), respectively; Figure S1). Finally, at hNET, MDMA and its analogs also elicited potent [^3H]MPP $^+$ release (Figure 1c, right panels), when compared with the negative and positive controls at this transporter (nisoxetine (30 μM) and (*S*)-amphetamine (10 μM), respectively; Figure S1). In this case, the net efflux at hNET was inferior to hSERT for all compounds, including their respective positive controls, suggesting a difference in reverse transport efficiency by these two transporters. Additionally, the potentiation of efflux caused by monensin was not significant at hNET. The calculated area under the curve of the percentage of [^3H]substrate released between 8 and 18 min ($\text{AUC}_{8-18\text{min}}$) better revealed the efflux differences between the conditions without (KHB; -) and with monensin (MON; +) for the positive and negative controls (Figure S1). Altogether, these results suggest that all compounds act as substrates/releasers at all monoamine transporters, with more efficiency and efficacy at hSERT.

3.3 | hSERT- and hDAT-mediated currents confirm full and partial substrate profiles

Since the DAT/SERT ratio of a given compound has been associated with its abuse liability (Baumann et al., 2011; Luethi & Liechti, 2020;

Simmler et al., 2013), we proceeded with a more detailed molecular characterization of MDMA and its analogs at these two transporters in order to better differentiate their substrate profile. For this, we performed electrophysiology using whole-cell patch-clamp configuration ($V_h = -60\text{mV}$) in HEK293 cells overexpressing either hSERT or hDAT. hSERT and hDAT are Na^+ dependent transporters, and the application of a substrate (but not an inhibitor) elicits an inward-directed steady-state current that persists for the whole application. Thus, it is currently used to identify whether a test drug acts as a substrate (Bhat et al., 2017; Hasenhuetl et al., 2019). At hSERT, the application of MDMA analogs elicited inwardly directed steady-state currents in a concentration-dependent manner that resembled those elicited by MDMA or 5-HT (Figure 2a,b). Non-linear regression of the concentration-response curve led to EC_{50} values in the low micromolar range ((in μM) 5-HT: $0.17 < \text{MDMA}$: $0.27 < \text{TDMA}$: $0.44 < \text{SeDMA}$: $0.77 < \text{ODMA}$: 1.27), and similar E_{MAX} values (5-HT: 94%; MDMA: 92.6%; TDMA: 93.2%; SeDMA 97.1%; ODMA: 109.5%). At hDAT, instead, all the compounds elicited inward-directed steady-state currents (Figure 2c,d), but their amplitude reached only 30–50% of the ones elicited by the saturating concentration of DA (30 μM). Non-linear regression revealed EC_{50} values in the low micromolar range (in μM ; MDMA: $2.51 < \text{ODMA}$: $3.97 < \text{TDMA}$: $4.29 < \text{SeDMA}$: $5.97 < \text{DA}$: 6.40) and similar E_{MAX} values (MDMA: 31.9%; ODMA: 48.2%; TDMA: 30.1%; SeDMA: 25.7%), except for DA (E_{max} : 104.1%). To rule out that the effect was not due to system bias, we measured transporter-mediated currents in *Xenopus laevis* oocytes expressing hSERT or hDAT, as previously described (Cao et al., 1998; Hilber et al., 2005 Meinild et al., 2004; Sonders et al., 1997; Sitte et al., 1998). Figure S2 shows the effects of either 5-HT/DA, MDMA, ODMA, and TDMA, on hSERT- and hDAT-mediated currents, respectively.

Collectively, our results from these experiments revealed that MDMA and its analogs: (1) interacted with hSERT and hDAT at a similar low micromolar range; (2) elicited strong hSERT- and moderate hDAT-mediated efflux, and (3) accordingly showed full-efficacy for eliciting hSERT-mediated steady-state currents but partial-efficacy for eliciting hDAT-mediated steady-state currents. Taken together, the data support the conclusion that MDMA and its analogs show a preference to act as full substrates at hSERT but as partial substrates at hDAT.

3.4 | The binding poses of MDMA and its analogs overlap with the natural substrate, both at hSERT and hDAT

To better investigate the full vs. partial substrate dichotomy and the binding of MDMA, ODMA, TDMA, and SeDMA to hSERT and hDAT structures, we performed molecular docking calculations. Notably, these compounds exhibited remarkably similar binding poses when compared to each other (Figure 3a,c), particularly when interacting with hSERT. The binding poses revealed that the positively charged amino group of the compounds faced the transmembrane helices forming the bundle domain (TM1, TM2, TM6, and TM7), while the

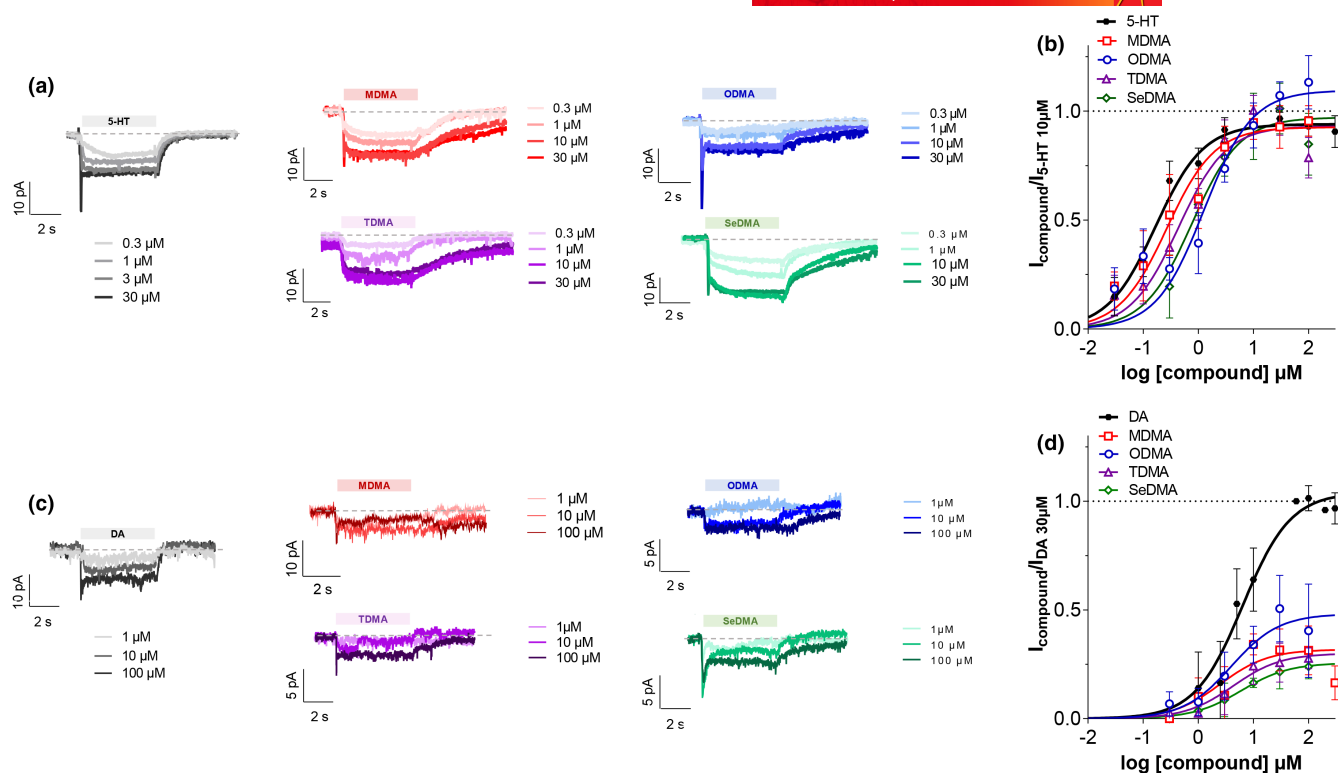


FIGURE 2 Measurement of transporter-mediated steady-state currents through whole-cell patch clamp (holding voltage (V_h) = -60 mV). (a) Representative single-cell traces showing hSERT-mediated currents elicited by increasing concentration of 5-hydroxytryptamine (5-HT; serotonin; gray), MDMA (red), ODMA (blue), TDMA (purple), and SeDMA (green). (b) Concentration-response curves at hSERT. Data were normalized to the steady-state current of the saturating concentration of 5-HT ($10 \mu\text{M}$) and plotted using non-linear regression. The half-maximal effective concentration (EC_{50}) values were extrapolated (5-HT: $0.17 \mu\text{M}$ < MDMA: $0.27 \mu\text{M}$ < TDMA: $0.44 \mu\text{M}$ < SeDMA: $0.77 \mu\text{M}$ < ODMA: $1.27 \mu\text{M}$) as well as the maximum effect (E_{MAX}) values (5-HT: 94%; MDMA: 92.6%; TDMA: 93.2%; SeDMA 97.1%; ODMA: 109.5%). (c) Representative single-cell traces showing hDAT-mediated currents elicited by increasing concentration of DA (gray), MDMA (red), ODMA (blue), TDMA (purple), and SeDMA (green). (d) Concentration-response curves at hDAT. Data were normalized to the steady-state current of the saturating concentration of DA ($30 \mu\text{M}$) and plotted using non-linear regression. The EC_{50} values were extrapolated (MDMA: $2.51 \mu\text{M}$ < ODMA: $3.97 \mu\text{M}$ < TDMA: $4.29 \mu\text{M}$ < SeDMA: $5.97 \mu\text{M}$ < DA: $6.40 \mu\text{M}$) as well as the E_{MAX} values (DA: 104.1%; MDMA: 31.9%; ODMA: 48.2%; TDMA: 30.1%; SeDMA: 25.7%). Data are mean \pm SD from two to seven individual cells per concentration ($n=2-7$).

aromatic ring system interacted with the scaffold domain (TM3, TM4, TM8, and TM9). This suggests that all ligands can interact with the same residues that interact with the endogenous substrates. Additionally, the observed conformations compare well with the 5-HT pose observed in hSERT structure (PDB ID: 7MGW; (Yang & Gouaux, 2021)) and the poses of dopamine and methamphetamine observed in the drosophila dDAT structures (PDB ID: 4XP1 and 4XP6; (Wang et al., 2015)). Furthermore, upon analyzing the interacting residues (Figure 3b,d (left and right panels); Figure S3), we observed that these compounds established polar interactions through their charged amino group, as well as non-polar interactions through their aromatic ring system. The charged amine group formed electrostatic and hydrogen bond interactions with the side-chain of both D98 and S438, respectively, at hSERT, and electrostatic and hydrogen bond interactions with the side-chain of D79 and the backbone of F320, respectively, at hDAT. Additionally, we noted that these compounds interacted with additional residues (marked with black stars) which have been shown to interact with 5-HT and dopamine (Wang et al., 2015; Yang & Gouaux, 2021) in hSERT and hDAT, respectively (Figure S3).

3.5 | MDMA activates 5-HT_{2A}, 5-HT_{2B} and 5-HT_{2C} receptors more potently than its analogs

To further investigate our compounds directly at monoaminergic receptors, we explored their activity at 5-HT₂ receptor subtypes, namely, 5-HT_{2A}, 5-HT_{2B}, and 5-HT_{2C} receptors. The activation of 5-HT_{2A}R has been linked to the mechanism of action of psychedelics (McClure-Begley & Roth, 2022). MDMA is known to be a weak 5-HT_{2A} receptor agonist (Nash et al., 1994), and this effect has been associated with its mesolimbic DA release and reinforcing properties (Orejarena et al., 2011; Teitler et al., 1990). Additionally, drugs causing valvular heart disease and primary pulmonary hypertension in humans have been found to share affinity for 5-HT_{2B} receptors (Launay et al., 2002; Rothman et al., 2000; Setola et al., 2003, 2005). MDMA has been shown to bind to and activate h5-HT_{2B} receptors with sub-micromolar affinity (Setola et al., 2003). Finally, 5-HT_{2C} agonists have been shown to decrease appetite (Thomsen et al., 2008).

To investigate the effect of MDMA and its analogs on 5-HT₂ receptor activity, we measured Gq dissociation directly using a BRET-based

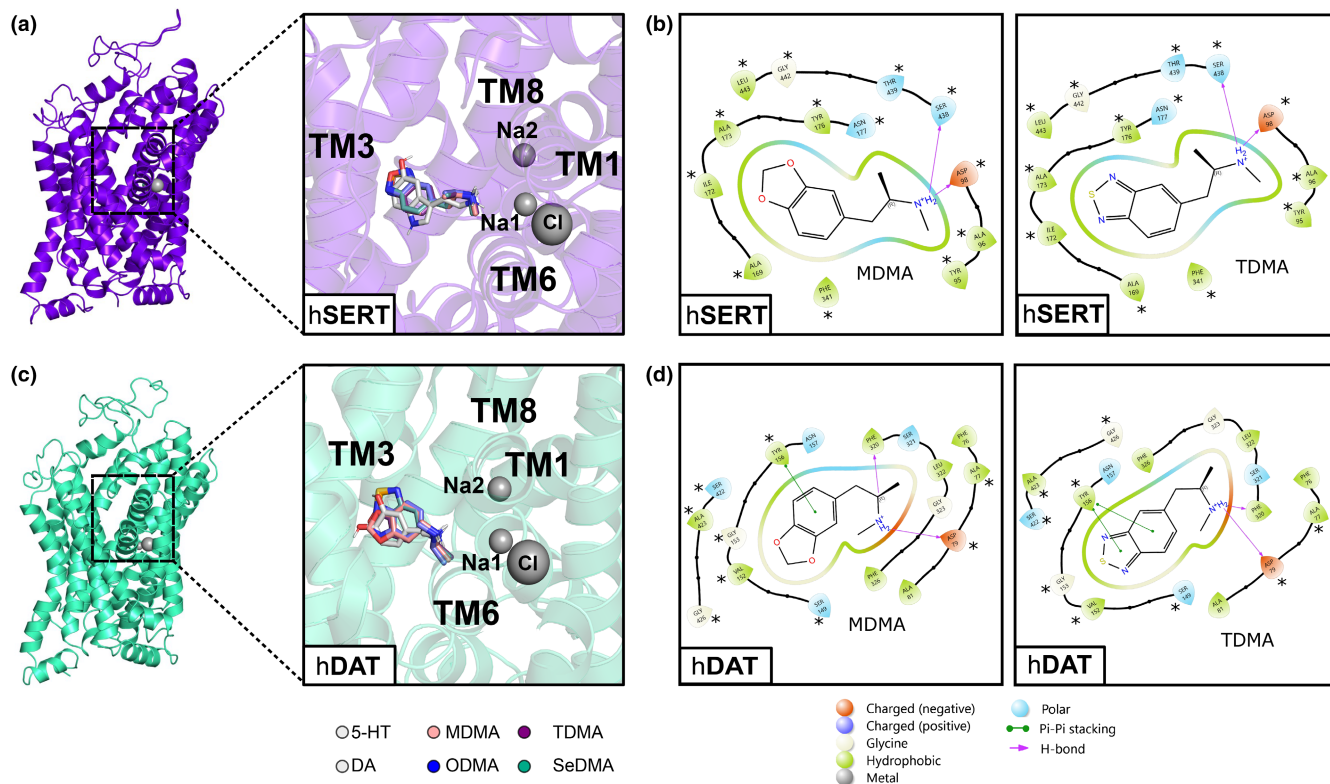


FIGURE 3 Molecular docking. (a, c) Outward-open structure of hSERT (purple) or hDAT (green cyan) and the binding poses of all ligands (the best pose of 10 independent docking runs) in each transporter. MDMA: salmon, OMDA: blue, TDMA: purple, SeDMA: green and both serotonin (5-HT) and dopamine (DA) in light gray. (b) Left and right panels show the 2D interaction scheme of MDMA and TDMA molecules, respectively, highlighting the main interactions with hSERT (obtained using Maestro version 13.6.122). (d) The left and right panels show the 2D interaction scheme of MDMA and TDMA molecules, respectively, highlighting the main interactions with hDAT (obtained using Maestro version 13.6.122). The asterisks indicate the residues that also interact with 5-HT in hSERT (PDB ID:7MGW) and with DA in dDAT (PDB ID:4XP1). The residues of the protein are shown like guitar picks linked together on a string. The orientation of the guitar pick must be read as: the guitar picks pointing away from the ligand means the backbone of that residue is facing towards the ligand, and when the guitar pick is pointing towards the ligand that means the side chain of that residue is facing the ligand.

assay system (Figure 4a,b; Cunningham et al., 2023; Lewis et al., 2023). In these assays, surface receptor expression was quantified using an anti-FLAG ELISA, which indicated 5-HT_{2A}, 5-HT_{2B} and 5-HT_{2C} receptors expressed similarly at the cell surface (Figure S4). Compared to MDMA, all three bioisosteres (ODMA, TDMA, and SeDMA) exhibited weaker potency (Figure 4c-f; Table 2) at 5-HT_{2A/2B/2C} Gq dissociation, with SeDMA being the weakest. In fact, all three bioisosteres were approximately 10-fold weaker to activate 5-HT_{2B/2C} receptors compared to MDMA. To complement these results, next we measured calcium flux responses using both a Fluo-4 calcium dye in a FLIPR-based measurement and a GcAMP6 reporter, which both assays showed that all 3 bioisosteric MDMA analogs weakly activate 5-HT_{2A}, 5-HT_{2B}, and 5-HT_{2C} receptors compared to MDMA (Figure S4). We further performed molecular docking studies of MDMA and its analogs at 5-HT receptors and observed that all the compounds show different binding poses within the same receptor, displaying different interaction patterns, although these differences are minimal at 5-HT_{2B} receptor. Additionally, the interaction between the charged amino group with the conserved aspartate residue (D155 in 5-HT_{2A}, D135 in 5-HT_{2B}, and D134 in 5-HT_{2C}) is consensus, apart from SeDMA at 5-HT_{2C} receptor,

where this interaction is replaced by interactions with S138 and W324 (Figure S6). Furthermore, when comparing the binding poses of the same molecule across different receptors, the evidence that these compounds interact differently is further confirmed (Figure S7).

3.6 | CYP-mediated N-demethylation is the only hepatic metabolic pathway shared between MDMA and its analogs

After examining effects on the monoaminergic targets, the impact of the bioisosteric replacements used in the design of the three MDMA analogs on in vitro hepatic metabolism was also investigated. Suitable in vitro systems can be used to mimic human metabolism. Such systems are pooled human liver microsomes (pHLM) combined with cytosol (pHLC) or pooled human liver S9 fraction (pS9), which are commonly used to identify phase I, but also phase II metabolites or both (Richter, Flockner, et al., 2017a). The S9 fraction usually contains cytosol and microsomes but the enzyme activities are usually lower than those of isolated

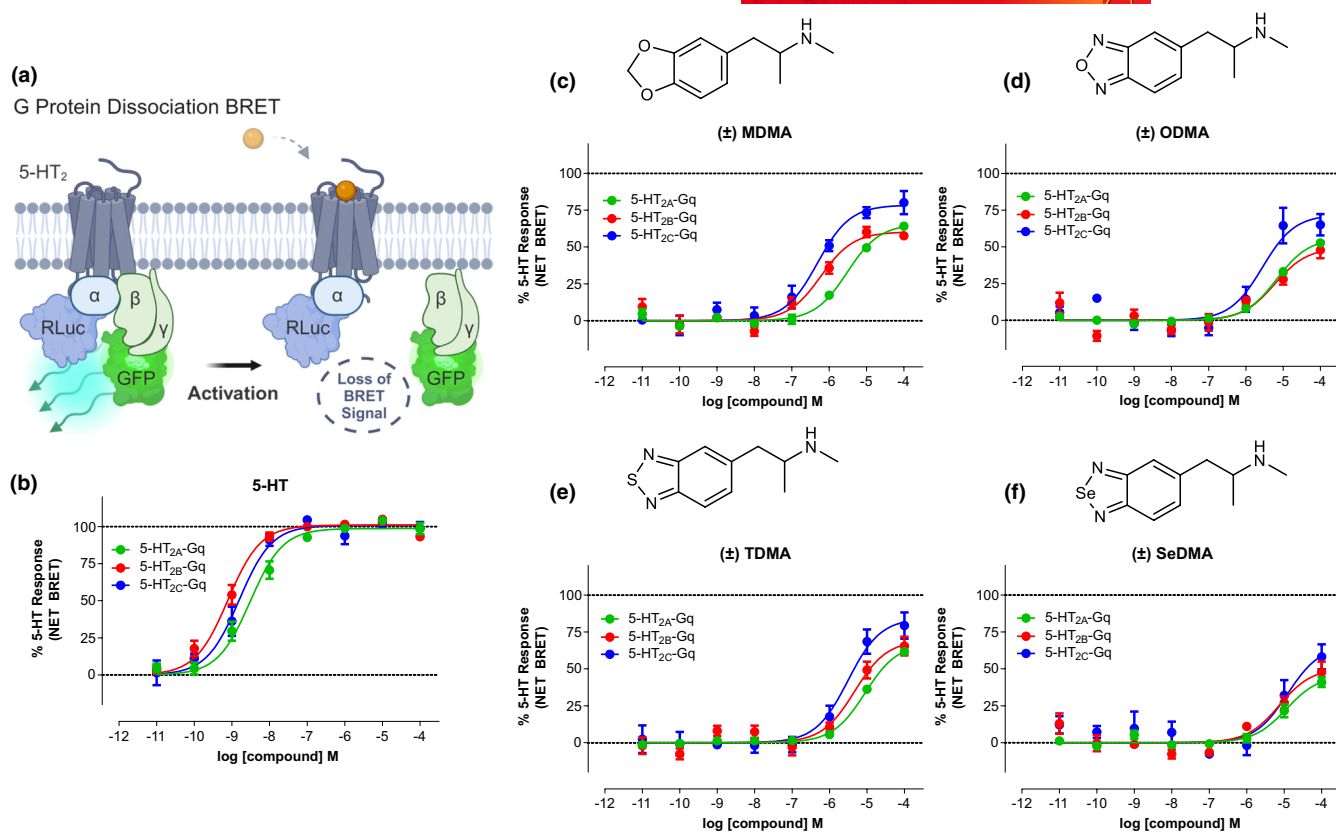


FIGURE 4 MDMA activates 5-HT_{2A}, 5-HT_{2B}, and 5-HT_{2C} receptors more potently than its analogs. (a) BRET Gq dissociation assay for human 5-HT₂ receptors (5-HT_{2A}-green, 5-HT_{2B}-red, 5-HT_{2C}-blue) using (b) 5-HT as positive control and measuring agonist activity of (c) MDMA compared to MDMA bioisosteric analogs (d) ODMA, (e) TDMA and (f) SeDMA. Data represent mean \pm SEM from three independent cell culture preparations ($n=3$).

TABLE 2 Gq dissociation BRET: 5-HT_{2A/2B/2C} receptor activity.

	5-HT _{2A}			5-HT _{2B}			5-HT _{2C}		
	EC ₅₀ (nM)	pEC ₅₀ (\pm SEM)	E _{max} % 5-HT (\pm SEM)	EC ₅₀ (nM)	pEC ₅₀ (\pm SEM)	E _{max} % 5-HT (\pm SEM)	EC ₅₀ (nM)	pEC ₅₀ (\pm SEM)	E _{max} % 5-HT (\pm SEM)
5-HT	3.04	8.52 \pm 0.07	100	0.78	9.11 \pm 0.06	100	1.56	8.81 \pm 0.09	100
(\pm) MDMA	3024	5.52 \pm 0.09	65.5 \pm 2.7	598	6.22 \pm 0.12	60.3 \pm 3.2	490	6.31 \pm 0.13	78.5 \pm 4.2
(\pm) ODMA	6714	5.17 \pm 0.07	56.1 \pm 2.3	5924	5.23 \pm 0.23	49.4 \pm 6.2	2755	5.56 \pm 0.20	71.9 \pm 7.0
(\pm) TDMA	8818	5.06 \pm 0.06	67.2 \pm 2.3	4631	5.33 \pm 0.16	69.4 \pm 5.8	3098	5.51 \pm 0.18	84.3 \pm 7.2
(\pm) SeMDA	11480	4.94 \pm 0.14	45.8 \pm 4.1	7434	5.13 \pm 0.22	50.6 \pm 6.5	12190	4.91 \pm 0.27	65.9 \pm 11.5

Note: 5-HT₂ Gq dissociation EC₅₀ and E_{MAX} parameter estimates of MDMA and analogs. 5-HT₂ activation was measured using Gq/γ9 dissociation by BRET. Data represent mean and SEM from three independent cell culture preparations ($n=3$) performed in duplicate and reflect Figure 4a-f.

microsomes or cytosol. Thus pHLM/pHLC is often tested besides pS9 (Brandon et al., 2003; Richter, Flockerzi, et al., 2017a; Rock & Foti, 2019). All metabolites of ODMA, TDMA, and SeDMA detected from incubations with pHLM or pS9 mixtures along with their metabolite identification number, calculated exact mass of protonated molecule, elemental composition, and retention time are given in Table 3. Metabolites were tentatively identified by comparison of their HRMS² spectra and fragmentation patterns of the parent compounds to those of the putative metabolites. All HRMS² spectra of tentatively identified metabolites are

shown in Figure S8 (ODMA), S9 (TDMA), and S10 (SeDMA). For ODMA, three phase I metabolites were detected in all incubations. Metabolic reactions included N-dealkylation (ODMA-M1), N-hydroxylation (ODMA-M2), and hydroxylation (ODMA-M3). For TDMA, two phase I metabolites were found in all incubations. Hence, metabolic reactions included N-dealkylation (TDMA-M1) and N-hydroxylation (TDMA-M2). Finally, for SeDMA, one phase I reaction, namely an N-hydroxylation (SeDMA-M2) was found in all incubations. No phase II metabolites could be detected for any MDMA analogs. Thus, in this study, the main metabolic pathways

TABLE 3 Pooled human liver microsomes/S9 fraction incubation for identification of phase I and II metabolites.

Metabolite-ID	Metabolic reaction	Calculated exact mass, <i>m/z</i>	Elemental composition	RT, min
ODMA	-	192.1131	C ₁₀ H ₁₄ N ₃ O	3.92
ODMA-M1	<i>N</i> -Dealkylation	178.0975	C ₉ H ₁₂ N ₃ O	4.56
ODMA-M2	<i>N</i> -Hydroxylation	208.0935	C ₁₀ H ₁₄ N ₃ O ₂	0.96
ODMA-M3	Hydroxylation at benzoxadiazole	208.1081	C ₁₀ H ₁₄ N ₃ O ₂	4.13
TDMA	-	208.0903	C ₁₀ H ₁₄ N ₃ S	3.89
TDMA-M1	<i>N</i> -Dealkylation	194.07464	C ₉ H ₁₂ N ₃ S	4.16
TDMA-M2	<i>N</i> -Hydroxylation	224.0852	C ₁₀ H ₁₄ N ₃ OS	1.04
SeDMA	-	256.0347	C ₁₀ H ₁₃ N ₃ Se	4.17
SeDMA-M1	<i>N</i> -Hydroxylation	272.0297	C ₁₀ H ₁₄ N ₃ OSe	1.16
MDMA	-	194.1176	C ₁₁ H ₁₅ NO ₂	N.A.
MDMA-M1 ^a	<i>N</i> -Dealkylation	180.1019	C ₁₀ H ₁₃ NO ₂	N.A.
MDMA-M2 ^a	Demethylenation	182.1176	C ₁₀ H ₁₅ NO ₂	N.A.
MDMA-M3 ^a	Demethylenation + methylation	196.1332	C ₁₁ H ₁₇ NO ₂	N.A.
MDMA-M4 ^a	Demethylenation + methylation	196.1332	C ₁₁ H ₁₇ NO ₂	N.A.
MDMA-M5 ^a	Demethylenation + sulfation	262.0744	C ₁₀ H ₁₅ NO ₅ S	N.A.
MDMA-M6 ^a	Demethylenation + sulfation	262.0744	C ₁₀ H ₁₅ NO ₅ S	N.A.
MDMA-M7 ^a	Demethylenation + methylation + sulfation	274.0755	C ₁₁ H ₁₇ NO ₅ S	N.A.

Note: Detection of ODMA, TDMA, and SeDMA and their phase I metabolites in pooled human liver microsomes and reported phase I and II metabolites of MDMA in literature in pooled human liver microsomes or S9 (Richter, Flockerzi, et al., 2017a; Schwaninger, Meyer, Zapp, & Maurer, 2011b) together with their metabolite identification numbers (ID), calculated the exact mass of the protonated molecule (M+H⁺), elemental composition and retention time (RT). Metabolites were sorted by increasing mass.

^aLiterature data, N.A., no retention time available for the used analytical method.

of all three MDMA bioisosteres in vitro were *N*-demethylation and/or *N*-hydroxylation (Figure 5a–c). Comparing the results against the in vitro metabolism of MDMA (Richter, Flockerzi, et al., 2017a; Schwaninger, Meyer, Barnes, et al., 2011a; Schwaninger, Meyer, Zapp, & Maurer, 2011b; Table 3; Figure 5d), only *N*-demethylation was a common transformation. In contrast to MDMA, the bioisosteric replacement used in ODMA, TDMA, and SeDMA does not allow for a demethylenation to occur, which prevents catechol formation and subsequent formation of corresponding phase II metabolites as seen with MDMA (Figure 5d).

3.7 | TDMA is the MDMA analog which is more susceptible to biotransformation

To further complement the previous results, we performed metabolic stability studies. Measuring the metabolic stability of MDMA and its analogs helps to evaluate their susceptibility to biotransformation and hence, part of their pharmacokinetic properties. Metabolic stability in pHLM incubation of each compound is shown in Figure 5e, and in vitro half-life ($t_{1/2}$) values, calculated microsomal intrinsic clearances (CL_{int,micr}), and intrinsic clearances (CL_{int}) are summarized in Table 4. Non-metabolic compound degradation during pHLM incubation could be excluded by control incubations as the *t*-test did not show a significant difference between parent compound

concentration after 150min in control incubation and initial concentration after 0min (MDMA: $p=0.3657$, $t=1.1603$, $df=2$; ODMA: $p=0.1957$, $t=1.9143$, $df=2$; TDMA: $p=0.9529$, $t=0.0666$, $df=2$; SeDMA: $p=0.1767$, $t=2.0513$, $df=2$). The in vitro half-lives were determined using a cut-off value of 150min, based on the decrease in enzyme activities after 2h of incubation (Baranczewski et al., 2006). Clearance values could not be calculated for ODMA, SeDMA, and MDMA as their half-lives were longer than 150min. The half-life of TDMA was 53min, resulting in a CL_{int} of 11.2mL/min/kg.

3.8 | Different CYPs are involved in the biotransformation of MDMA analogs

The involvement of different cytochrome P450 isozymes in the transformation of MDMA analogs was also analyzed. Mapping of isozymes is essential for predicting potential interactions, e.g., between drugs, or interindividual variations due to different expressions of isozymes. Therefore, the involvement of 10 different CYP isozymes and FMO3 in the phase I biotransformation of ODMA, TDMA, and SeDMA was investigated using a monooxygenase activity screening. Results of isozyme mapping of initial phase I metabolites compared to pHLM incubations of ODMA, TDMA, and SeDMA are summarized in Table 5. The absence of interfering compounds was confirmed by blank incubations.

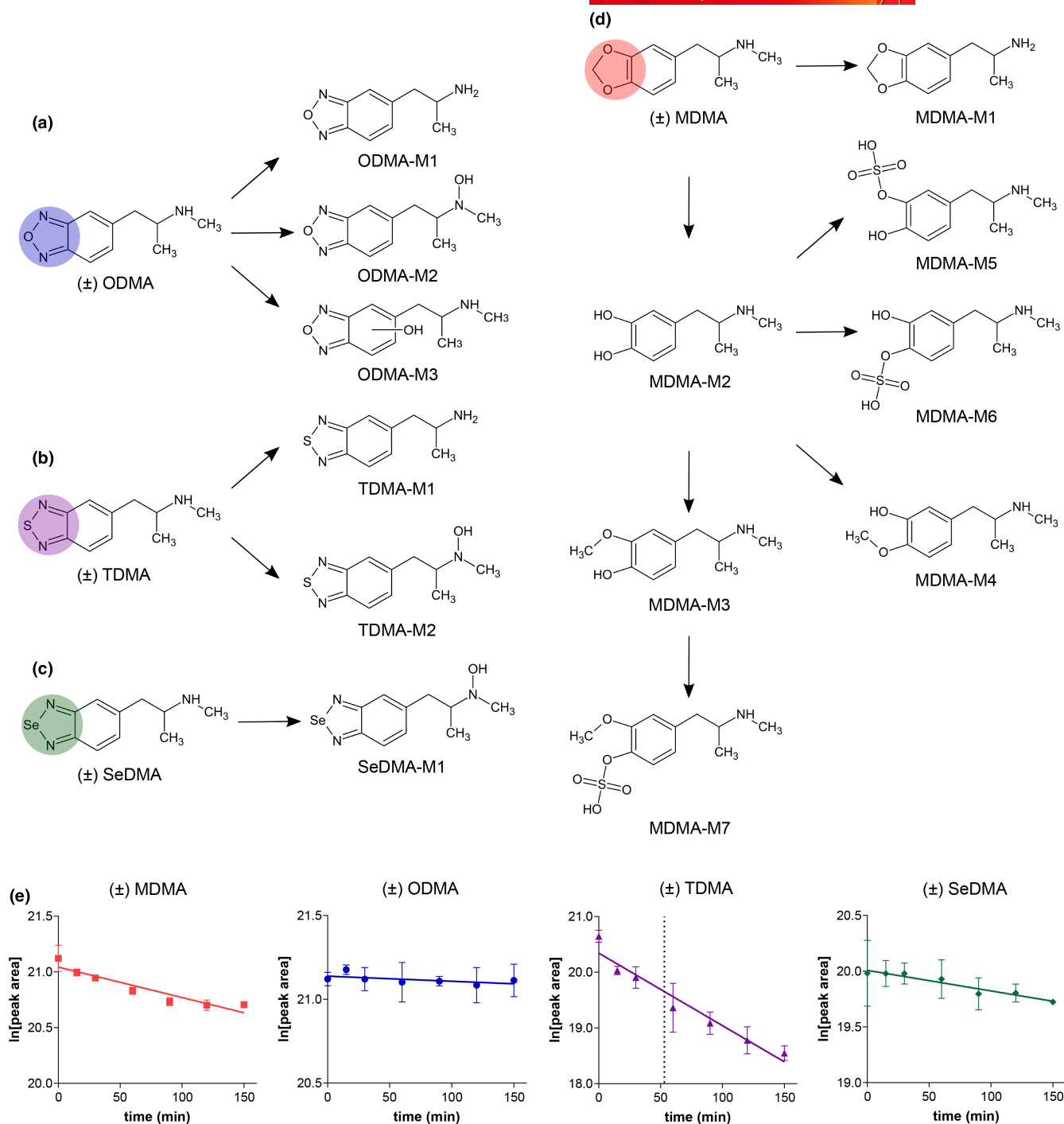


FIGURE 5 MDMA and its analogs differ in their hepatic metabolism. (a–c) Metabolic pathways of ODMA, TDMA, and SeDMA in incubations with pooled human liver microsomes. Undefined hydroxylation position is indicated by unspecific bonds. Metabolite-IDs correspond to Table 3. (d) Metabolic pathways of MDMA reported in the literature in incubations with pooled human liver microsomes and/or S9 fraction (Richter, Flockerzi, et al., 2017a; Schwaninger, Meyer, Zapp, & Maurer, 2011b). Metabolite-IDs correspond to Table 3. (e) Metabolic stability of MDMA (red), ODMA (blue), TDMA (purple), and SeDMA (green) in incubations with pooled human liver microsomes (pHLM). Incubation time is plotted versus the natural logarithm of the peak area of the compound. Points indicate mean \pm SD from two independent incubations with pHLM ($n=2$), $t_{1/2}$ = in vitro half-life.

3.9 | Interaction profiles of MDMA and bioisosteric analogs with hOCT1, hOCT2, and hPMAT

In previous studies, we have found that a range of psychoactive substances differentially interact with the low-affinity high-capacity

transporters (Angenoorth et al., 2021; Maier, Niello, et al., 2021a; Mayer et al., 2018). Thus, to complement our studies on hepatic metabolism, we further investigated whether MDMA and its analogs were able to interact with the human organic cation transporters (hOCTs) 1 (hOCT1), 2 (hOCT2), and 3 (hOCT3), and human

plasma membrane monoamine transporter (hPMAT). hOCT1-3, and hPMAT are generally involved in the uptake and elimination of various endogenous compounds, including monoamines, as well as of xenobiotics, such as drugs and toxins. They are expressed both in peripheral organs (e.g. liver and kidney) and in the central nervous system, playing a major role in maintaining monoaminergic homeostasis (Hayer-Zillgen et al., 2002; Koepsell, 2020). Thus, the interaction profile of the tested compounds was explored in hOCTs and hPMAT, and the respective IC_{50} values were calculated (Figure 6; Table 6). In brief, MDMA and its analogs displayed IC_{50} values in the low micromolar range at hOCT1, hOCT2, and hPMAT, although SeDMA displayed a reduced inhibitory potential of the [3H]MPP⁺ uptake at hOCT-2 compared to its congeners ($IC_{50} = 68.3 \pm 30.5$). Moreover, neither MDMA nor its congeners interacted with hOCT3 in a physiologically relevant concentration (IC_{50} values $\geq 696.2 \pm 57.0 \mu M$). Finally, at hPMAT, all compounds displayed IC_{50} values in the low micromolar range. In sum, MDMA analogs showed weaker interactions and displayed minor pharmacological differences in relation to uptake inhibition at hOCT1, hOCT2 and hPMAT, when compared with MDMA.

TABLE 4 Metabolic stability of ODMA, TDMA, SeDMA, and MDMA in pooled human liver microsomes (pHLM) incubations expressed as in vitro half-life ($t_{1/2}$) and calculated microsomal intrinsic clearance ($CL_{int,micr}$) and intrinsic clearance (CL_{int}).

	$t_{1/2}$ (min)	$CL_{int,micr}$ (mL/min/mg)	CL_{int} (mL/min/kg)
(±) MDMA	>150	-	-
(±) ODMA	>150	-	-
(±) TDMA	53	0.0131	11.2
(±) SeDMA	>150	-	-

TABLE 5 Isozyme mapping of initial ODMA, TDMA, and SeDMA metabolites in comparison to pooled human liver microsomes (pHLM) and flavin-containing monooxygenase (FMO) 3 incubations.

Metabolite ID	pHLM	CYP										FMO 3
		1A2	2A6	2B6	2C8	2C9	2C19	2D6	2E1	3A4	3A5	
ODMA												
ODMA-M1 (N-Dealkyl)	+	+	-	+	-	-	+	+	-	+	-	-
ODMA-M2 (N-Hydroxy)	+	+	-	+	-	-	+	+	-	+	-	+
ODMA-M3 (Hydroxy)	+	-	-	-	-	-	-	+	-	+	-	-
TDMA												
TDMA-M1 (N-Dealkyl)	+	+	-	+	-	-	+	+	-	+	-	-
TDMA-M2 (N-Hydroxy)	+	+	-	+	-	-	+	+	-	+	-	+
SeDMA												
SeDMA-M1 (N-Hydroxy)	+	+	-	-	-	-	+	+	-	-	-	+
MDMA												
N-Dealkyl*	+	+	-	+	-	-	+	+	-	+	+	/
Demethylenyl*	+	+	-	+	-	-	+	+	-	+	+	/

Note: Metabolite-IDs correspond to Table 1. Isozyme mapping of MDMA metabolites reported in the literature (Kraemer & Maurer, 2002; Maurer et al., 2000; Meyer et al., 2008). Cytochrome P450 (CYP); *, literature data; +, detected; -, not detected; /, not described in literature.

4 | DISCUSSION

Effective and long-lasting pharmacotherapies for specific neuropsychiatric disorders, including PTSD, continue to be important medical needs. Current therapies for PTSD include psychotherapy and/or pharmacotherapy, with selective serotonin reuptake inhibitors (SSRI) being the first-line agents (Williams et al., 2022). However, SSRIs show low efficacy in reducing PTSD symptoms severity (Hoskins et al., 2015; Williams et al., 2022). Recently, there has been a growing interest in psychedelics and other psychoactive drugs as possible therapeutic agents for the treatment of a range of psychiatric disorders (De Vos et al., 2021). In this context, MDMA is emerging as a candidate for the treatment of PTSD in combination with psychotherapy (Mitchell et al., 2021, 2023; Mithoefer et al., 2011, 2018).

In this study, we investigated three new MDMA analogs and showed that, compared to MDMA, they: (1) mimic its interaction with the high-affinity low-capacity monoamine transporters, setting off their reverse transport mode, and displaying a full substrate profile at hSERT, but a partial substrate profile at hDAT; (2) are less potent and efficacious at 5-HT_{2A/2B/2C} receptors; (3) differ in their hepatic metabolism, sharing only N-demethylation during phase I without the formation of phase II metabolites; (4) have similar metabolic stabilities, except TDMA, which displays a reduced $t_{1/2}$, $CL_{int,micr}$ and CL_{int} ; (5) interact slightly less potently with the low-affinity high-capacity transporters hOCT1, hOCT2, and hPMAT.

The therapeutic effects of MDMA involve a complex interplay between pharmacological and psychological effects. However, one of the key pharmacological mechanisms include the substrate-like activity and efflux-induction at monoamine transporters. Specifically, MDMA is a substrate at SERT that reverses its transport and leads to potent 5-HT release both in vitro and in vivo

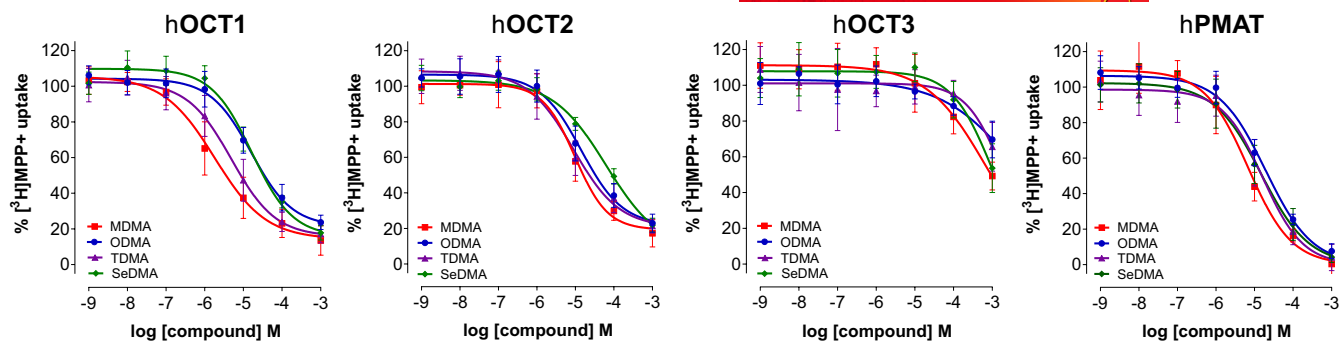


FIGURE 6 MDMA and its analogs interact with the low-affinity high-capacity human organic cation transporters (hOCT1-3) and human plasma membrane monoamine transporter (hPMAT) at low micromolar concentrations. Uptake-inhibition curves at hOCT1, hOCT2, hOCT3, and hPMAT. Curves were plotted and fitted by non-linear regression, and data were best fitted to a sigmoidal dose-response curve to obtain IC_{50} values (see Table 6). Data are mean \pm SD from three to four independent cell culture preparations ($n=3-4$), performed in triplicate.

TABLE 6 Uptake inhibition assays.

	$[^3H]MPP^+$ uptake, IC_{50} (μM) hOCT1	$[^3H]MPP^+$ uptake, IC_{50} (μM) hOCT2	$[^3H]MPP^+$ uptake, IC_{50} (μM) hOCT3	$[^3H]MPP^+$ uptake, IC_{50} (μM) hPMAT
(\pm) MDMA	2.8 ± 2.1	10.2 ± 4.6	696.2 ± 114.0	6.8 ± 3.9
(\pm) ODMA	17.4 ± 7.8	15.0 ± 7.4	2327 ± 888.7	20.2 ± 4.8
(\pm) TDMA	5.4 ± 2.2	19.1 ± 18.7	2407 ± 1342	17.0 ± 8.3
(\pm) SeDMA	16.4 ± 2.8	68.3 ± 30.5	1130 ± 682.5	22.0 ± 18.8

Note: The potency of MDMA and its analogs ODMA, TDMA, and SeDMA at hOCT1, hOCT2, hOCT3, and hPMAT. Data represent mean and SD from at least three independent cell culture preparations ($n \geq 3$) performed in triplicate.

(Green et al., 2003; Montgomery et al., 2007; Rudnick & Wall, 1992; Sandtner et al., 2016; Steinkellner et al., 2011). At NET, while in vitro studies have shown that MDMA leads to equally potent or superior transporter-mediated NE release, in vivo studies have been inconclusive due to the lack of microdialysis studies for this monoamine (Dunlap et al., 2018; Green et al., 2003; Selken & Nichols, 2007; Verrico et al., 2007). Nevertheless, MDMA-induced increase in plasma NE levels has been strongly associated with its cardiotoxic and psychostimulant effects (Hysek et al., 2011). At DAT, most studies show that MDMA is also able to induce DA release both in vitro and in vivo, although this effect appears to be less pronounced (Baumann et al., 2012; Johnson et al., 1986). Regarding MDMA's psychological effects, a part of its therapeutic action has been associated with its prosocial effects. Interestingly, in mice, the interaction of MDMA with SERT-containing 5-HT terminals in the nucleus accumbens has been demonstrated to be necessary and sufficient to explain this effect, whereas its non-social drug reward has been associated to the DA signaling in this same brain region (Heifets et al., 2019; Walsh et al., 2018, 2023).

In the current study, we used heterologous expressing systems to evaluate the pharmacological mechanisms in greater detail and developed novel MDMA analogs. We have found that both MDMA and its analogs interacted with monoamine transporters at low micromolar concentrations with minor differences in their IC_{50} values (Table 1). Similar IC_{50} values have previously been reported for MDMA under comparable experimental conditions (Ilic et al., 2020; Luethi et al., 2019; Maier et al., 2018;

Montgomery et al., 2007). Subsequent release assays showed that MDMA and its analogs induced potent hSERT-mediated $[^3H]5-HT$ release and hNET-mediated $[^3H]MPP^+$ release, whereas a moderate hDAT-mediated $[^3H]MPP^+$ release. At hSERT and hDAT, these data were further substantiated by whole-cell patch-clamp in HEK293 cells and two-electrode voltage-clamp in *Xenopus laevis* oocytes, which also confirmed that MDMA and its analogs elicit increasing concentration-dependent steady-state currents at hSERT and hDAT. Considering the amplitude of the currents at hSERT and hDAT, our findings suggest that MDMA and its analogs work as full substrates at hSERT, but as partial substrates at hDAT. Furthermore, molecular docking studies have shown that MDMA and its analogs display similar binding poses when binding at hSERT or hDAT (Figure 3a,c). This result shows that the MDMA analogs preserve the same interaction pattern as MDMA despite the bioisosteric substitution of the methylenedioxy group. Interestingly, at hSERT, all interacting residues were shared between the compounds and 5-HT (Figure 3b, Figure S3). However, at hDAT, the compounds interacted with a larger number of residues compared to DA (Figure 3d, Figure S3). Such finding is particularly significant as it suggests that the docked compounds have a higher potential to mimic the binding of the native substrate in hSERT compared to hDAT, which is most likely a consequence of the higher structural similarity of these compounds to 5-HT as compared to dopamine, and supports our results with hSERT substrate preference over hDAT. The partial efficacy at hDAT might arise from slow binding kinetics, as shown already for the hSERT



partial substrate PAL-1045 (Bhat et al., 2017). Further studies will be necessary to evaluate the extent to which binding kinetics might be involved in the pharmacodynamics of the novel MDMA analogs, and whether slow binding kinetics might play a role for their in vivo effects as shown already for a range of other psychoactive substances (Niello et al., 2023).

Given the unique psychopharmacological profile of MDMA, many other studies have explored the molecular pharmacology of other MDMA analogs, enantiomers, and/or metabolites at monoamine transporters (Dolan et al., 2019; Kolaczynska et al., 2022; Luethi et al., 2019; Montgomery et al., 2007; Pitts et al., 2018; Sandtner et al., 2016; Shimshoni et al., 2017). To our knowledge, this is the first study that investigated three novel MDMA analogs that reflected a bioisosteric replacement of the methylenedioxy group of MDMA and their impact on key molecular targets, together with a concomitant analysis of their hepatic metabolism.

In our study, these bioisosteric MDMA analogs exhibited less potent and efficacious agonist activity at 5-HT_{2A} and almost a 10-fold less potent activity at activating 5-HT_{2B} and 5-HT_{2C} receptors. For 5-HT_{2A}, a weaker interaction with this receptor could translate into a reduced potential for mesolimbic DA release and reinforcing properties, together with a reduction/loss of the hallucinogenic potential of these compounds at higher doses (Orejarena et al., 2011; Teitler et al., 1990). Further studies will be necessary to confirm the reduced hallucinogenic effects in vivo, especially in relation to the 5-HT_{2A} signaling pathways that might be involved (Wallach et al., 2023). Importantly, the weaker agonism at the 5-HT_{2B} receptor by the MDMA analogs suggests an improved pharmacological profile for the analogs with respect to MDMA, especially regarding the risk for cardiotoxicity. Nevertheless, taking into account their interaction profile with hNET, the evaluation of risk for cardiotoxic effects with these novel MDMA bioisosteric analogs is still warranted. Additional molecular docking studies have shown that MDMA and its analogs display different binding poses within each receptor 5-HT₂ subtype, and hence, different interaction patterns, supporting the fact that minor chemical modifications such as bioisosteric replacements might translate to different molecular interactions only in specific targets.

The hepatic metabolism studies showed that *N*-demethylation was the only metabolic pathway shared between MDMA and its analogs. The ring systems present in ODMA, TDMA, and SeDMA did not appear to undergo ring opening, in contrast to MDMA known to show demethylation reactions and formation of catechol and subsequent phase II metabolites. Thus, our data support the hypothesis that the investigated MDMA analogs might be less likely to generate free radicals, in contrast with MDMA. Since demethylation cannot occur, further studies are required to investigate whether this will impact on their pharmacokinetic properties. In this context, metabolic stability screenings were performed to all test compounds to estimate their susceptibility to biotransformation (Baranczewski et al., 2006). Thus, the depletion of the compounds during incubation with pHLM was used to determine metabolic stability, which was expressed as $t_{1/2}$, $CL_{int,micr}$ and CL_{int} .

The latter was calculated by scaling CL_{micr} to whole liver dimensions. CL_{int} is defined as the maximum activity of the liver towards a drug in the absence of other physiological determinants such as hepatic blood flow and drug binding within the blood mixture (Baranczewski et al., 2006). To ensure the absence of non-specific protein binding, protein concentrations should be minimized and the concentration of the compound during incubation should be below the Michaelis–Menten concentration (K_m). Since no information on K_m values was available for the tested compounds, a low compound concentration was used in the assay as recommended by Baranczewski et al. (Baranczewski et al., 2006). Non-metabolic degradation of the substances could be excluded by control incubations without pHLM and subsequent *t*-test, which showed no significant differences in the natural logarithms of the peak area of incubations after 0 min and control incubations. According to McNaney et al. (McNaney et al., 2008) TDMA could be classified as an intermediate clearance compound. On the other hand, MDMA, ODMA, and SeDMA showed only weak metabolic degradation, as half-life and clearance value could not be determined.

Regarding the isozyme mapping, several CYPs participated in the transformation of the MDMA analogs. Since ODMA and TDMA were mainly metabolized by CYP3A4, increased drug levels and intoxications may result from CYP3A4 inhibition, e.g., due to drug–drug or drug–food interactions (DDIs or DFIs, respectively). However, due to additional involvement of CYP2D6 in the metabolism of all three compounds, inhibition of CYP3A4 is expected to be less substantial in CYP2D6 poor metabolizers. In addition to CYP3A4 and CYP2D6, CYP1A2 was also involved in the phase I biotransformation of ODMA, TDMA, and SeDMA, which may prevent an increase in drug levels caused by CYP3A4 inhibitors or in CYP2D6 poor metabolizers. The *N*-demethylation catalyzed by CYP1A2 and CYP2D6 was also reported for MDMA (Kraemer & Maurer, 2002; Maurer et al., 2000; Meyer et al., 2008), leading to 3,4-methylenedioxyamphetamine (MDA). Since MDMA is known to be a substrate of CYP2D6 that can lead to its autoinhibition (De La Torre et al., 2004), and that it displayed a long in vitro half-life in our metabolic stability studies, further studies are encouraged to address this issue with these novel analogs to understand their potential of displaying DDIs or DFIs.

OCT1 and OCT2 play essential roles in drug pharmacokinetics, pharmacodynamics, and DDIs (Zhou et al., 2021), since they are involved in mediating hepatic uptake and renal secretion, respectively, of a wide range of cationic drugs (Suo et al., 2023). Overall, MDMA analogs demonstrated weaker interactions and minor pharmacological differences in relation to their uptake inhibition at OCT1, OCT2, and PMAT, compared with MDMA, which suggests a potentially reduced risk for DDIs. None of the compounds interacted with OCT3 at relevant physiological concentrations.

Overall, these data suggest that ODMA, TDMA, and SeDMA are compounds that: (1) are capable of mimicking part of the MDMA molecular interactions at relevant physiological targets, such as the monoamine transporters; (2) have lower activity and show different molecular interaction patterns at 5-HT_{2A}, 5-HT_{2B} and 5-HT_{2C}



receptors, and (3) show improved metabolic properties, being TDMA the compound that is more susceptible to biotransformation. When compared with MDMA, further studies are needed to assess whether the favorable off-target profiles identified in this study translate to novel drug candidates with reduced side effect profiles. Particularly, *in vitro* and *in silico* studies should include an assessment of the interaction of these MDMA bioisosteres resulting metabolites at 5-HT₂ receptors, and *in vivo* studies should include behavioral pharmacology in rodents.

AUTHOR CONTRIBUTIONS

Ana Sofia Alberto-Silva: Investigation; writing – original draft; validation; visualization; formal analysis; writing – review and editing. **Selina Hemmer:** Formal analysis; investigation; validation; visualization; writing – original draft. **Hailey A. Bock:** Investigation; formal analysis; validation; visualization; writing – original draft. **Leticia Alves da Silva:** Formal analysis; writing – original draft; validation; visualization; investigation. **Kenneth R. Scott:** Investigation; formal analysis; methodology. **Nina Kastner:** Investigation; formal analysis. **Manan Bhatt:** Formal analysis; investigation. **Marco Niello:** Methodology; writing – review and editing. **Kathrin Jäntschi:** Investigation. **Oliver Kudlacek:** Methodology; writing – review and editing. **Elena Bossi:** Supervision; writing – review and editing; funding acquisition. **Thomas Stockner:** Supervision; writing – review and editing; funding acquisition. **Markus R. Meyer:** Writing – review and editing; supervision. **John D. McCorvy:** Supervision; writing – review and editing; funding acquisition. **Simon D. Brandt:** Conceptualization; writing – review and editing. **Pierce Kavanagh:** Conceptualization; formal analysis; investigation; methodology; validation; visualization. **Harald H. Sitte:** Conceptualization; writing – review and editing; funding acquisition; supervision.

ACKNOWLEDGMENTS

This project has received funding from the European Union's Horizon 2020 research and innovation programme under the Marie Skłodowska-Curie grant agreement No: 860954 (to TS, HHS, and EB). We gratefully acknowledge support by the Austrian Science Fund/FWF standalone project P35589 (to HHS and MN), P32017 (to TS), and the doctoral programme W1232 (MolTag). In addition, the project received support by the National Institutes of Health Grant R01 MH133849 (to JDM).

CONFLICT OF INTEREST STATEMENT

The authors declare no conflict of interest.

PEER REVIEW

The peer review history for this article is available at <https://www.webofscience.com/api/gateway/wos/peer-review/10.1111/jnc.16149>.

DATA AVAILABILITY STATEMENT

The data that support the findings of this study are available from the corresponding author upon reasonable request.

ORCID

Ana Sofia Alberto-Silva <https://orcid.org/0000-0001-5662-0581>
 Selina Hemmer <https://orcid.org/0009-0009-5534-0612>
 Hailey A. Bock <https://orcid.org/0000-0002-3457-9319>
 Leticia Alves da Silva <https://orcid.org/0000-0002-9620-3974>
 Kenneth R. Scott <https://orcid.org/0009-0009-5113-7908>
 Nina Kastner <https://orcid.org/0000-0002-1576-9029>
 Manan Bhatt <https://orcid.org/0000-0002-5792-0081>
 Marco Niello <https://orcid.org/0000-0002-0518-5791>
 Oliver Kudlacek <https://orcid.org/0000-0002-3086-8551>
 Elena Bossi <https://orcid.org/0000-0002-9549-2153>
 Thomas Stockner <https://orcid.org/0000-0002-7071-8283>
 Markus R. Meyer <https://orcid.org/0000-0003-4377-6784>
 John D. McCorvy <https://orcid.org/0000-0001-7555-9413>
 Simon D. Brandt <https://orcid.org/0000-0001-8632-5372>
 Pierce Kavanagh <https://orcid.org/0000-0002-1613-3305>
 Harald H. Sitte <https://orcid.org/0000-0002-1339-7444>

REFERENCES

- Abdel-Magid, A. F., Carson, K. G., Harris, B. D., Maryanoff, C. A., & Shah, R. D. (1996). Reductive amination of aldehydes and ketones with weakly basic anilines using sodium triacetoxyborohydride. *The Journal of Organic Chemistry*, 61, 3849–3862.
- Angenoorth, T. J. F., Stankovic, S., Niello, M., Holy, M., Brandt, S. D., Sitte, H. H., & Maier, J. (2021). Interaction profiles of central nervous system active drugs at human organic cation transporters 1–3 and human plasma membrane monoamine transporter. *International Journal of Molecular Sciences*, 22, 1–16.
- Anzali, S., Mederski, W. W. K. R., Osswald, M., & Dorsch, D. (1997). Endothelin antagonists: Search for surrogates of methylenedioxyphenyl by means of a Kohonen neural network. *Bioorganic & Medicinal Chemistry Letters*, 8, 11–16.
- Baranczewski, P., Stańczyk, A., Sundberg, K., Svensson, R., Wallin, Å., Jansson, J., Garberg, P., & Postlind, H. (2006). Introduction to *in vitro* estimation of metabolic stability and drug interactions of new chemical entities in drug discovery and development. *Pharmacological Reports*, 58, 453–472.
- Baumann, M. H., Ayestas, M. A., Partilla, J. S., Sink, J. R., Shulgin, A. T., Daley, P. F., Brandt, S. D., Rothman, R. B., Ruoho, A. E., & Cozzi, N. V. (2012). The designer methcathinone analogs, mephedrone and methylone, are substrates for monoamine transporters in brain tissue. *Neuropsychopharmacology*, 37, 1192–1203.
- Baumann, M. H., Clark, R. D., Woolverton, W. L., Wee, S., Blough, B. E., & Rothman, R. B. (2011). *In vivo* effects of amphetamine analogs reveal evidence for serotonergic inhibition of mesolimbic dopamine transmission in the rat. *The Journal of Pharmacology and Experimental Therapeutics*, 337, 218–225.
- Bhat, S., Hasenhuettl, P. S., Kasture, A., Ali, E. K., Baumann, M. H., Blough, B. E., Susic, S., Sandtner, W., & Freissmuth, M. (2017). Conformational state interactions provide clues to the pharmacochaperone potential of serotonin transporter partial substrates. *The Journal of Biological Chemistry*, 292, 16773–16786.
- Bhatt, M., Iacovo, A., Di, R. T., Roseti, C., Cinquetti, R., & Bossi, E. (2022). The “www” of *Xenopus laevis* oocytes: The why, when, what of *Xenopus laevis* oocytes in membrane transporters research. *Membranes (Basel)*, 12, 927.
- Bhattacharyya, S., Schapira, A. H., Mikhailidis, D. P., & Davar, J. (2009). Drug-induced fibrotic valvular heart disease. *Lancet*, 374, 577–585.
- Brandon, E. F. A., Raap, C. D., Meijerman, I., Beijnen, J. H., & Schellens, J. H. M. (2003). An update on *in vitro* test methods in human hepatic



- drug biotransformation research: Pros and cons. *Toxicology and Applied Pharmacology*, 189, 233–246.
- Briner, K., Burkhardt, J. P., Burkholder, T. P., Fisher, M. J., Gritton, W. H., Kohlman, D. T., Liang, S. X., Miller, S. C., Mullaney, J. T., & Xu, Y. (2000). Aminoalkylbenzofurans as serotonin (5-HT_{2C}) agonists.
- Cao, Y., Li, M., Mager, S., & Lester, H. A. (1998). Amino acid residues that control pH modulation of transport-associated current in mammalian serotonin transporters. *The Journal of Neuroscience*, 18, 7739–7749.
- Capela, J. P., Meisel, A., Abreu, A. R., Branco, P. S., Ferreira, L. M., Lobo, A. M., Remião, F., Bastos, M. L., & Carvalho, F. (2006a). Neurotoxicity of ecstasy metabolites in rat cortical neurons, and influence of hyperthermia. *The Journal of Pharmacology and Experimental Therapeutics*, 316, 53–61.
- Capela, J. P., Ruscher, K., Lautenschlager, M., Freyer, D., Dirnagl, U., Gaio, A. R., Bastos, M. L., Meisel, A., & Carvalho, F. (2006b). Ecstasy-induced cell death in cortical neuronal cultures is serotonin 2A-receptor-dependent and potentiated under hyperthermia. *Neuroscience*, 139, 1069–1081.
- Chen, T. W., Wardill, T. J., Sun, Y., Pulver, S. R., Renninger, S. L., Baohan, A., Schreiter, E. R., Kerr, R. A., Orger, M. B., Jayaraman, V., Looger, L. L., Svoboda, K., & Kim, D. S. (2013). Ultrasensitive fluorescent proteins for imaging neuronal activity. *Nature*, 499, 295–300.
- Coleman, J. A., Green, E. M., & Gouaux, E. (2016). X-ray structures and mechanism of the human serotonin transporter. *Nature*, 532, 334–339.
- Cunningham, M. J., Bock, H. A., Serrano, I. C., Bechand, B., Vidyadhara, D. J., Bonniwell, E. M., Lankri, D., Duggan, P., Nazarova, A. L., Cao, A. B., Calkins, M. M., Khirsariya, P., Hwu, C., Katritch, V., Chandra, S. S., McCorvy, J. D., & Sames, D. (2023). Pharmacological mechanism of the non-hallucinogenic 5-HT_{2A} agonist Ariadne and Analogs. *ACS Chemical Neuroscience*, 14, 119–135.
- Davies, B., & Morris, T. (1993). Physiological parameters in laboratory animals and humans. *Pharmaceutical Research*, 10(7), 1093–1095.
- De Vos, C. M. H., Mason, N. L., & Kuypers, K. P. C. (2021). Psychedelics and neuroplasticity: A systematic review unraveling the biological underpinnings of psychedelics. *Frontiers in Psychiatry*, 12, 724606.
- Delaforge, M., Jaouen, M., & Bouille, G. (1999). Inhibitory metabolite complex formation of methylenedioxymethamphetamine with rat and human cytochrome P450. Particular involvement of CYP 2D. *Environmental Toxicology and Pharmacology*, 7, 153–158.
- Dinger, J., Meyer, M. R., & Maurer, H. H. (2016). In vitro cytochrome P450 inhibition potential of methylenedioxy-derived designer drugs studied with a two-cocktail approach. *Archives of Toxicology*, 90, 305–318.
- Dolan, S. B., Chen, Z., Huang, R., Gatch, M. B., & Worth, F. (2019). “Ecstasy” to addiction: Mechanisms and reinforcing effects of three synthetic cathinone analogs of MDMA. *Neuropharmacology*, 133, 171–180.
- Dunlap, L. E., Andrews, A. M., & Olson, D. E. (2018). Dark classics in chemical neuroscience: 3,4-methylenedioxymethamphetamine. *ACS Chemical Neuroscience*, 9, 2408–2427.
- Esteban, B., O’Shea, E., Camarero, J., Sanchez, V., Green, A. R., & Colado, M. I. (2001). 3,4-methylenedioxymethamphetamine induces monoamine release, but not toxicity, when administered centrally at a concentration occurring following a peripherally injected neurotoxic dose. *Psychopharmacology*, 154, 251–260.
- Fonseca, D. A., Ribeiro, D. M., Tapadas, M., & Cotrim, M. D. (2021). Ecstasy (3,4-methylenedioxymethamphetamine): Cardiovascular effects and mechanisms. *European Journal of Pharmacology*, 903, 174156.
- Gadakh, B., Vondenhoff, G., Lescrinier, E., Rozenski, J., Froeyen, M., & Van Aerschot, A. (2014). Base substituted 5'-O-(N-isoleucyl)sulfamoyl nucleoside analogues as potential antibacterial agents. *Bioorganic & Medicinal Chemistry*, 22, 2875–2886.
- Gampfer, T. M., Richter, L. H. J., Schäper, J., Wagmann, L., & Meyer, M. R. (2019). Toxicokinetics and analytical toxicology of the abused opioid U-48800—In vitro metabolism, metabolic stability, isozyme mapping, and plasma protein binding. *Drug Testing and Analysis*, 11, 1572–1580.
- Giros, B., Mestikawy, S., El, G. N., Zheng, K., Han, H., Yang-Feng, T., & Caron, M. G. (1992). Cloning, pharmacological characterization, and chromosome assignment of the human dopamine transporter. *Molecular Pharmacology*, 42, 383–390.
- Gradisch, R., Szollosi, D., Niello, M., Lazzarin, E., Sitte, H. H., & Stockner, T. (2022). Occlusion of the human serotonin transporter is mediated by serotonin-induced conformational changes in the bundle domain. *The Journal of Biological Chemistry*, 298, 1–14.
- Green, A. R., Mehan, A. O., Elliott, J. M., O’Shea, E., & Colado, M. I. (2003). The pharmacology and clinical pharmacology of 3,4-methylenedioxymethamphetamine (MDMA, “ecstasy”). *Pharmacological Reviews*, 55, 463–508.
- Hasenhuetl, P. S., Bhat, S., Freissmuth, M., & Sandtner, W. (2019). Functional selectivity and partial efficacy at the monoamine transporters: A unified model of allosteric modulation and amphetamine-induced substrate release. *Molecular Pharmacology*, 95, 303–312.
- Hasenhuetl, P. S., Bhat, S., Mayer, F. P., Sitte, H. H., Freissmuth, M., & Sandtner, W. (2018). A kinetic account for amphetamine-induced monoamine release. *The Journal of General Physiology*, 150, 431–451.
- Hayer-Zillgen, M., Brüss, M., & Bönisch, H. (2002). Expression and pharmacological profile of the human organic cation transporters hOCT1, hOCT2 and hOCT3. *British Journal of Pharmacology*, 136, 829–836.
- Heifets, B. D., Salgado, J. S., Taylor, M. D., Hoerbelt, P., Cardozo, P. D. F., Steinberg, E. E., Walsh, J. J., Sze, J. Y., & Malenka, R. C. (2019). Distinct neural mechanisms for the prosocial and rewarding properties of MDMA. *Science Translational Medicine*, 11, 1–11.
- Hilber, B., Scholze, P., Dorostkar, M. M., Sandtner, W., Holy, M., Boehm, S., Singer, E. A., & Sitte, H. H. (2005). Serotonin-transporter mediated efflux: A pharmacological analysis of amphetamines and non-amphetamines. *Neuropharmacology*, 49(6), 811–819. <https://doi.org/10.1016/j.neuropharm.2005.08.008>
- Hoskins, M., Pearce, J., Bethell, A., Dankova, L., Barbui, C., Tol, W. A., van Ommeren, M., de Jong, J., Seedat, S., Chen, H., & Bisson, J. I. (2015). Pharmacotherapy for post-traumatic stress disorder: Systematic review and meta-analysis. *The British Journal of Psychiatry*, 206, 93–100.
- Hysek, C. M., Simmler, L. D., Ineichen, M., Grouzmann, E., Hoener, M. C., Brenneisen, R., Huwyler, J., & Liechti, M. E. (2011). The norepinephrine transporter inhibitor reboxetine reduces stimulant effects of MDMA (ecstasy) in humans. *Clinical Pharmacology and Therapeutics*, 90, 246–255.
- Ilic, M., Holy, M., Jaentsch, K., Liechti, M. E., Lubec, G., Baumann, M. H., Sitte, H. H., & Luethi, D. (2020). Cell-based radiotracer binding and uptake inhibition assays: A comparison of in vitro methods to assess the potency of drugs that target monoamine transporters. *Frontiers in Pharmacology*, 11, 1–11.
- Jayanthi, S., Ladenheim, B., Andrews, A. M., & Cadet, J. L. (1999). Overexpression of human copper/zinc superoxide dismutase in transgenic mice attenuates oxidative stress caused by methylenedioxymethamphetamine (ecstasy). *Neuroscience*, 91, 1379–1387.
- Johnson, M. P., Hoffman, A. J., & Nichols, D. E. (1986). Effects of enantiomers of MDA, MDMA and related analogues on [3H]serotonin and [3H]dopamine release from superfused rat brain slices. *European Journal of Pharmacology*, 132, 269–276.
- Jones, G., Willett, P., Glen, R. C., Leach, A. R., & Taylor, R. (1997). Development and validation of a genetic algorithm for flexible docking. *Journal of Molecular Biology*, 267, 727–748.
- Koepsell, H. (2020). Organic cation transporters in health and disease. *Pharmacological Reviews*, 72, 253–319.
- Kolaczynska, K. E., Ducret, P., Trachsel, D., Hoener, M. C., Liechti, M. E., & Luethi, D. (2022). Pharmacological characterization



- of 3,4-methylenedioxyamphetamine (MDA) analogs and two amphetamine-based compounds: α -DEPEA and DPIA. *European Neuropsychopharmacology*, 59, 9–22.
- Kraemer, T., & Maurer, H. H. (2002). Toxicokinetics of amphetamines: Metabolism and toxicokinetic data of designer drugs, amphetamine, methamphetamine, and their N-alkyl derivatives. *Therapeutic Drug Monitoring*, 24, 277–289.
- Kroeze, W. K., Sassano, M. F., Huang, X.-P., Lansu, K., McCorvy, J. D., Giguère, P. M., Sciaky, N., & Roth, B. L. (2015). PRESTO-Tango as an open-source resource for interrogation of the druggable human GPCRome. *Nature Structural & Molecular Biology*, 22, 362–369.
- La Torre, R., De, F. M., Roset, P. N., Pizarro, N., Abanades, S., Segura, M., Segura, J., & Camí, J. (2004). Human pharmacology of MDMA: Pharmacokinetics, metabolism, and disposition. *Therapeutic Drug Monitoring*, 26, 137–144.
- Launay, J. M., Hervé, P., Peoc'h, K., Tournois, C., Callebert, J., Nebigil, C. G., Etienne, N., Drouet, L., Humbert, M. S., & Maroteaux, G. L. (2002). Function of the serotonin 5-hydroxytryptamine 2B receptor in pulmonary hypertension. *Nature Medicine*, 8, 1129–1135.
- Lewis, V., Bonniwell, E. M., Lanham, J. K., Ghaffari, A., Sheshbaradaran, H., Cao, A. B., Calkins, M. M., Bautista-Carro, M. A., Arsenault, E., Telfer, A., Taghavi-Abkuh, F. F., Malcolm, N. J., el Sayegh, F., Abizaid, A., Schmid, Y., Morton, K., Halberstadt, A. L., Aguilar-Valles, A., & McCorvy, J. D. (2023). A non-hallucinogenic LSD analog with therapeutic potential for mood disorders. *Cell Reports*, 42, 112203.
- Luethi, D., Kolaczynska, K. E., Walter, M., Suzuki, M., Rice, K. C., Blough, B. E., Hoener, M. C., Baumann, M. H., & Liechti, M. E. (2019). Metabolites of the ring-substituted stimulants MDMA, methylone and MDPV differentially affect human monoaminergic systems. *Journal of Psychopharmacology*, 33, 831–841.
- Luethi, D., & Liechti, M. E. (2020). *Designer drugs: Mechanism of action and adverse effects*. Springer.
- Maier, J., Mayer, F. P., Luethi, D., Holy, M., Jäntschi, K., Reither, H., Hirtler, L., Hoener, M. C., Liechti, M. E., Piffl, C., Brandt, S. D., & Sitte, H. H. (2018). The psychostimulant (\pm)-cis-4,4'-dimethylaminorex (4,4'-DMAR) interacts with human plasmalemmal and vesicular monoamine transporters. *Neuropharmacology*, 138, 282–291.
- Maier, J., Niello, M., Rudin, D., Daws, L. C., & Sitte, H. H. (2021a). The interaction of organic cation transporters 1-3 and PMAT with psychoactive substances. In L. C. Daws (Ed.), *Handbook of experimental pharmacology*, (Vol. 266, pp. 199–214). Springer Nature.
- Maier, J., Rauter, L., Rudin, D., Niello, M., Holy, M., Schmid, D., Wilson, J., Blough, B. E., Gannon, B. M., Murnane, K. S., & Sitte, H. H. (2021b). α -PPP and its derivatives are selective partial releasers at the human norepinephrine transporter: A pharmacological characterization of interactions between pyrrolidinopropiophenones and uptake1 and uptake2 monoamine transporters. *Neuropharmacology*, 190, 108570.
- Maurer, H. H., Bickeboeller-Friedrich, J., Kraemer, T., & Peters, F. T. (2000). Toxicokinetics and analytical toxicology of amphetamine-derived designer drugs ('Ecstasy'). *Toxicology Letters*, 112–113, 133–142.
- Mayer, F. P., Luf, A., Nagy, C., Holy, M., Schmid, R., Freissmuth, M., & Sitte, H. H. (2016). Application of a combined approach to identify new psychoactive street drugs and decipher their mechanisms at monoamine transporters. *Current Topics in Behavioral Neurosciences*, 32, 333–350.
- Mayer, F. P., Niello, M., Cintulova, D., Sideromenos, S., Maier, J., Li, Y., Bulling, S., Kudlacek, O., Schicker, K., Iwamoto, H., Deng, F., Wan, J., Holy, M., Katamish, R., Sandtner, W., Li, Y., Pollak, D. D., Blakely, R. D., Mihovilovic, M. D., ... Sitte, H. H. (2023). Serotonin-releasing agents with reduced off-target effects. *Molecular Psychiatry*, 28, 722–732.
- Mayer, F. P., Schmid, D., Owens, W. A., Gould, G. G., Apuschkin, M., Kudlacek, O., Salzer, I., Boehm, S., Chiba, P., Williams, P. H., Wu, H. H., Gether, U., Koek, W., Daws, L. C., & Sitte, H. H. (2018). An unsuspected role for organic cation transporter 3 in the actions of amphetamine. *Neuropsychopharmacology*, 43, 2408–2417.
- McClure-Begley, T. D., & Roth, B. L. (2022). The promises and perils of psychedelic pharmacology for psychiatry. *Nature Reviews Drug Discovery*, 21, 463–473.
- McNaney, C. A., Drexler, D. M., Hnatyshyn, S. Y., Zvyaga, T. A., Knipe, J. O., Belcastro, J. V., & Sanders, M. (2008). An automated liquid chromatography-mass spectrometry process to determine metabolic stability half-life and intrinsic clearance of drug candidates by substrate depletion. *Assay and Drug Development Technologies*, 6, 121–129.
- Meanwell, N. A. (2014). The influence of bioisosteres in drug design: Tactical applications to address developability problems. *Current Topics in Medicinal Chemistry*, 9, 283–382.
- Meinild, A. K., Sitte, H. H., & Gether, U. (2004). Zinc potentiates an uncoupled anion conductance associated with the dopamine transporter. *The Journal of Biological Chemistry*, 279, 49671–49679.
- Meyer, M. R., Peters, F. T., & Maurer, H. H. (2008). The role of human hepatic cytochrome P450 isozymes in the metabolism of racemic 3,4-methylenedioxyethylamphetamine and its single enantiomers. *Drug Metabolism and Disposition*, 37, 1152–1156.
- Mitchell, J. M., Bogenschutz, M., Lilienstein, A., Harrison, C., Kleiman, S., Parker-Guilbert, K., Ot'alora G, M., Garas, W., Paleos, C., Gorman, I., Nicholas, C., Mithoefer, M., Carlin, S., Poulter, B., Mithoefer, A., Quevedo, S., Wells, G., Klaire, S. S., van der Kolk, B., ... Doblin, R. (2021). MDMA-assisted therapy for severe PTSD: a randomized, double-blind, placebo-controlled phase 3 study. *Nature Medicine*, 27, 1025–1033.
- Mitchell, J. M., Ot'alora G, M., van der Kolk, B., Shannon, S., Bogenschutz, M., Gelfand, Y., Paleos, C., Nicholas, C. R., Quevedo, S., Balliett, B., Hamilton, S., Mithoefer, M., Kleiman, S., Parker-Guilbert, K., Tzarfaty, K., Harrison, C., de Boer, A., Doblin, R., Yazar-Klosinski, B., & MAPP2 Study Collaborator Group. (2023). MDMA-assisted therapy for moderate to severe PTSD: a randomized, placebo-controlled phase 3 trial. *Nature Medicine*, 29, 2473–2480.
- Mithoefer, M. C., Mithoefer, A. T., Feduccia, A. A., Jerome, L., Wagner, M., Wymer, J., Holland, J., Hamilton, S., Yazar-Klosinski, B., Emerson, A., & Doblin, R. (2018). 3,4-methylenedioxymethamphetamine (MDMA)-assisted psychotherapy for post-traumatic stress disorder in military veterans, firefighters, and police officers: A randomized, double-blind, dose-response, phase 2 clinical trial. *The Lancet Psychiatry*, 5, 486–497.
- Mithoefer, M. C., Wagner, M. T., Mithoefer, A. T., Jerome, L., & Doblin, R. (2011). The safety and efficacy of \pm 3,4-methylenedioxymethamphetamine-assisted psychotherapy in subjects with chronic, treatment-resistant posttraumatic stress disorder: The first randomized controlled pilot study. *Journal of Psychopharmacology*, 25, 439–452.
- Montgomery, T., Buon, C., Eibauer, S., Guiry, P. J., Keenan, A. K., & McBean, G. J. (2007). Comparative potencies of 3,4-methylenedioxyamphetamine (MDMA) analogues as inhibitors of [3H]noradrenaline and [3H]5-HT transport in mammalian cell lines. *British Journal of Pharmacology*, 152, 1121–1130.
- Nadal-Gratacós, N., Alberto-Silva, A. S., Rodríguez-Soler, M., Urquiza, E., Espinosa-Velasco, M., Jäntschi, K., Holy, M., Batllori, X., Berzosa, X., Pubill, D., Camarasa, J., Sitte, H. H., Escubedo, E., & López-Arnau, R. (2021). Structure-activity relationship of novel second-generation synthetic cathinones: Mechanism of action, locomotion, reward, and immediate-early genes. *Frontiers in Pharmacology*, 12, 1–14.
- Nash, J. F., Roth, B. L., Brodtkin, J. D., Nichols, D. E., & Gudelsky, G. A. (1994). Effect of the R(-) and S(+) isomers of MDA and MDMA on phosphatidylinositol turnover in cultured cells expressing 5-HT_{2A} or 5-HT_{2C} receptors. *Neuroscience Letters*, 177, 111–115.
- Nichols, D. E. (1986). Differences between the mechanism of action of MDMA, MBDB, and the classic hallucinogens. Identification of a



- new therapeutic class: Entactogens. *Journal of Psychoactive Drugs*, 18, 305–313.
- Niello, M., Sideromenos, S., Gradisch, R., O Shea, R., Schwazer, J., Maier, J., Kastner, N., Sandtner, W., Jäntschi, K., Lupica, C. R., Hoffman, A. F., Lubec, G., Loland, C. J., Stockner, T., Pollak, D. D., Baumann, M. H., & Sitte, H. H. (2023). Persistent binding at dopamine transporters determines sustained psychostimulant effects. *Proceedings of the National Academy of Sciences of the United States of America*, 120, e2114204120.
- Orejarena, M. J., Lanfumey, L., Maldonado, R., & Robledo, P. (2011). Involvement of 5-HT_{2A} receptors in MDMA reinforcement and cue-induced reinstatement of MDMA-seeking behaviour. *The International Journal of Neuropsychopharmacology*, 14, 927–940.
- Paris, J. M., & Cunningham, K. A. (1992). Lack of serotonin neurotoxicity after intraraphe microinjection of (+)-3,4-methylenedioxyamphetamine (MDMA). *Brain Research Bulletin*, 28, 115–119.
- Pitts, E. G., Curry, D. W., Hampshire, K. N., Young, M. B., & Howell, L. L. (2018). (±)-MDMA and its enantiomers: Potential therapeutic advantages of R(-)-MDMA. *Psychopharmacology*, 235, 377–392.
- Richter, L. H. J., Flockerzi, V., Maurer, H. H., & Meyer, M. R. (2017a). Pooled human liver preparations, HepaRG, or HepG2 cell lines for metabolism studies of new psychoactive substances? A study using MDMA, MDDP, butylone, MDPPP, MDPV, MDPB, 5-MAPB, and 5-API as examples. *Journal of Pharmaceutical and Biomedical Analysis*, 143, 32–42.
- Richter, L. H. J., Kaminski, Y. R., Noor, F., Meyer, M. R., & Maurer, H. H. (2016). Metabolic fate of desomorphine elucidated using rat urine, pooled human liver preparations, and human hepatocyte cultures as well as its detectability using standard urine screening approaches. *Analytical and Bioanalytical Chemistry*, 408, 6283–6294.
- Richter, L. H. J., Maurer, H. H., & Meyer, M. R. (2017b). New psychoactive substances: Studies on the metabolism of XLR-11, AB-PINACA, FUB-PB-22, 4-methoxy- α -PVP, 25-I-NBOMe, and meclonazepam using human liver preparations in comparison to primary human hepatocytes, and human urine. *Toxicology Letters*, 280, 142–150.
- Rock, B. M., & Foti, R. S. (2019). Pharmacokinetic and drug metabolism properties of novel therapeutic modalities. *Drug Metabolism and Disposition*, 47, 1097–1099.
- Rothman, R. B., Baumann, M. H., Dersch, C. M., Romero, D. V., Rice, K. C., Carroll, F. I., & Partilla, J. S. (2001). Amphetamine-type central nervous system stimulants release norepinephrine more potently than they release dopamine and serotonin. *Synapse*, 39, 32–41.
- Rothman, R. B., Baumann, M. H., Savage, J. E., Rauser, L., McBride, A., Hufeisen, S. J., & Roth, B. L. (2000). Evidence for possible involvement of 5-HT_{2B} receptors in the cardiac valvulopathy associated with fenfluramine and other serotonergic medications. *Circulation*, 102, 2836–2841.
- Rudnick, G., & Wall, S. C. (1992). The molecular mechanism of “ecstasy” [3,4-methylenedioxy-methamphetamine (MDMA)]: Serotonin transporters are targets for MDMA-induced serotonin release. *Proceedings of the National Academy of Sciences of the United States of America*, 89, 1817–1821.
- Šali, A., & Blundell, T. L. (1993). *Comparative protein modelling by satisfaction of spatial restraints*.
- Sandtner, W., Stockner, T., Hasenhuetl, P. S., Partilla, J. S., Seddik, A., Zhang, Y. W., Cao, J., Holy, M., Steinkellner, T., Rudnick, G., Baumann, M. H., Ecker, G. F., Newman, A. H., & Sitte, H. H. (2016). Binding mode selection determines the action of ecstasy homologs at monoamine transporters. *Molecular Pharmacology*, 89, 165–175.
- Scholze, P., Zwach, J., Kattinger, A., Piffl, C., Singer, E. A., & Sitte, H. H. (2000). Transporter-mediated release: A superfusion study on human embryonic kidney cells stably expressing the human serotonin transporter. *The Journal of Pharmacology and Experimental Therapeutics*, 293, 870–878.
- Schwaninger, A. E., Meyer, M. R., Barnes, A. J., Kolbrich-Spargo, E. A., Gorelick, D. A., Goodwin, R. S., Huestis, M. A., & Maurer, H. H. (2011a). Urinary excretion kinetics of 3,4-methylenedioxyamphetamine (MDMA, ecstasy) and its phase I and phase II metabolites in humans following controlled MDMA administration. *Clinical Chemistry*, 57, 1748–1756.
- Schwaninger, A. E., Meyer, M. R., Zapp, J., & Maurer, H. H. (2011b). Sulfation of the 3,4-methylenedioxyamphetamine (MDMA) metabolites 3,4-dihydroxymethamphetamine (DHMA) and 4-hydroxy-3-methoxymethamphetamine (HMMA) and their capability to inhibit human sulfotransferases. *Toxicology Letters*, 202, 120–128.
- Selken, J., & Nichols, D. E. (2007). α 1-adrenergic receptors mediate the locomotor response to systemic administration of (±)-3,4-methylenedioxyamphetamine (MDMA) in rats. *Pharmacology, Biochemistry, and Behavior*, 86, 622–630.
- Setola, V., Dukat, M., Glennon, R. A., & Roth, B. L. (2005). Molecular determinants for the interaction of the valvulopathic anorexigen norfenfluramine with the 5-HT_{2B} receptor. *Molecular Pharmacology*, 68, 20–33.
- Setola, V., Hufeisen, S. J., Grande-Allen, K. J., Vesely, I., Glennon, R. A., Blough, B., Rothman, R. B., & Roth, B. L. (2003). 3,4-methylenedioxyamphetamine (MDMA, “ecstasy”) induces fenfluramine-like proliferative actions on human cardiac valvular interstitial cells in vitro. *Molecular Pharmacology*, 63, 1223–1229.
- Shankaran, M., Yamamoto, B. K., & Gudelsky, G. A. (1999). Mazindol attenuates the 3,4-methylenedioxyamphetamine-induced formation of hydroxyl radicals and long-term depletion of serotonin in the striatum. *Journal of Neurochemistry*, 72, 2516–2522.
- Shimshoni, J. A., Winkler, I., Golan, E., & Nutt, D. (2017). Neurochemical binding profiles of novel indole and benzofuran MDMA analogues. *Naunyn-Schmiedeberg's Archives of Pharmacology*, 390, 15–24.
- Shulgin, A. T., & Nichols, D. E. (1978). Characterization of three new psychotomimetics. In R. C. Stillman, & R. E. Willette (Eds.), *The psychopharmacology of hallucinogens* (pp. 74–83). Pergamon Press.
- Simmler, L. D., Buser, T. A., Donzelli, M., Schramm, Y., Dieu, L. H., Huwyler, J., Chaboz, S., Hoener, M. C., & Liechti, M. E. (2013). Pharmacological characterization of designer cathinones in vitro. *British Journal of Pharmacology*, 168, 458–470.
- Sitte, H. H., Huck, S., Reither, H., Boehm, S., Singer, E. A., & Piffl, C. (1998). Carrier-mediated release, transport rates, and charge transfer induced by amphetamine, tyramine, and dopamine in mammalian cells transfected with the human dopamine transporter. *Journal of Neurochemistry*, 71, 1289–1297.
- Sonders, M. S., Zhu, S. J., Zahniser, N. R., Kavanaugh, M. P., & Amara, S. G. (1997). Multiple ionic conductances of the human dopamine transporter: The actions of dopamine and psychostimulants. *The Journal of Neuroscience*, 17, 960–974.
- Steinkellner, T., Freissmuth, M., Sitte, H. H., & Montgomery, T. (2011). The ugly side of amphetamines: Short- and long-term toxicity of 3,4-methylenedioxyamphetamine (MDMA, ‘ecstasy’), methamphetamine and d-amphetamine. *Biological Chemistry*, 392, 103–115.
- Suo, Y., Wright, N. J., Guterres, H., Fedor, J. G., Butay, K. J., Borgnia, M. J., Im, W., & Lee, S. Y. (2023). Molecular basis of polyspecific drug and xenobiotic recognition by OCT1 and OCT2. *Nature Structural & Molecular Biology*, 30, 1001–1011.
- Szöllösi, D., & Stockner, T. (2021). Investigating the mechanism of sodium binding to SERT using direct simulations. *Frontiers in Cellular Neuroscience*, 15, 1–11.
- Teitler, M., Leonhardt, S., Appel, N. M., De Souza, E. B., & Glennon, R. A. (1990). Receptor pharmacology of MDMA and related hallucinogens. *Annals of the New York Academy of Sciences*, 600, 626–638.
- Thomsen, W. J., Grottick, A. J., Menzaghi, F., Reyes-Saldana, H., Espitia, S., Yuskin, D., Whelan, K., Martin, M., Morgan, M., Chen, W., al-Shamma, H., Smith, B., Chalmers, D., & Behan, D. (2008). Lorcaserin, a novel selective human 5-hydroxytryptamine_{2C} agonist: In vitro and in vivo pharmacological characterization. *The Journal of Pharmacology and Experimental Therapeutics*, 325, 577–587.
- Vacca, F., Gomes, A. S., Murashita, K., Cinquetti, R., Roseti, C., Barca, A., Rønnestad, I., Verri, T., & Bossi, E. (2022). Functional



- characterization of Atlantic salmon (*Salmo salar* L.) PepT2 transporters. *The Journal of Physiology*, 600, 2377–2400.
- Verrico, C. D., Miller, G. M., & Madras, B. K. (2007). MDMA (ecstasy) and human dopamine, norepinephrine, and serotonin transporters: Implications for MDMA-induced neurotoxicity and treatment. *Psychopharmacology*, 189, 489–503.
- Vizeli, P., Schmid, Y., Prestin, K., Meyer zu Schwabedissen, H. E., & Liechti, M. E. (2017). Pharmacogenetics of ecstasy: CYP1A2, CYP2C19, and CYP2B6 polymorphisms moderate pharmacokinetics of MDMA in healthy subjects. *European Neuropsychopharmacology*, 27, 232–238.
- Vollenweider, F. X., Gamma, A., Liechti, M., & Huber, T. (1998). Psychological and cardiovascular effects and short-term sequelae of MDMA ('Ecstasy') in MDMA-naïve healthy volunteers. *Neuropsychopharmacology*, 19, 241–251.
- Wagmann, L., Manier, S. K., Eckstein, N., Maurer, H. H., & Meyer, M. R. (2020). Toxicokinetic studies of the four new psychoactive substances 4-chloroethcathinone, N-ethylnorpentylone, N-ethylhexedrone, and 4-fluoro-alpha-pyrrolidinohexiophenone. *Forensic Toxicology*, 38, 59–69.
- Wagmann, L., Meyer, M. R., & Maurer, H. H. (2016). What is the contribution of human FMO3 in the N-oxygenation of selected therapeutic drugs and drugs of abuse? *Toxicology Letters*, 258, 55–70.
- Wallach, J., Cao, A. B., Calkins, M. M., Heim, A. J., Lanham, J. K., Bonniwell, E. M., Hennessey, J. J., Bock, H. A., Anderson, E. I., Sherwood, A. M., Morris, H., de Klein, R., Klein, A. K., Cuccurazzu, B., Gamrat, J., Fannana, T., Zauhar, R., Halberstadt, A. L., & McCorvy, J. D. (2023). Identification of 5-HT2A receptor signaling pathways responsible for psychedelic potential. *bioRxiv*, 2023.07.29.551106.
- Walsh, J. J., Christoffel, D. J., Heifets, B. D., Ben-Dor, G. A., Selimbeyoglu, A., Hung, L. W., Deisseroth, K., & Malenka, R. C. (2018). 5-HT release in nucleus accumbens rescues social deficits in mouse autism model. *Nature*, 560, 589–594.
- Walsh, J. J., Christoffel, D. J., & Malenka, R. C. (2023). Neural circuits regulating prosocial behaviors. *Neuropsychopharmacology*, 48, 79–89.
- Wang, K. H., Penmatsa, A., & Gouaux, E. (2015). Neurotransmitter and psychostimulant recognition by the dopamine transporter. *Nature*, 521, 322–327.
- Welter, J., Meyer, M. R., Wolf, E., Weinmann, W., Kavanagh, P., & Maurer, H. H. (2013). 2-Methiopropamine, a thiophene analogue of methamphetamine: Studies on its metabolism and detectability in the rat and human using GC-MS and LC-(HR)-MS techniques. *Analytical and Bioanalytical Chemistry*, 405, 3125–3135.
- Williams, T., Phillips, N. J., Stein, D. J., & Ipser, J. C. (2022). Pharmacotherapy for post traumatic stress disorder (PTSD). *The Cochrane Database of Systematic Reviews*, 3, CD002795.
- Yang, D., & Gouaux, E. (2021). Illumination of serotonin transporter mechanism and role of the allosteric site. *Science Advances*, 7, 1–11.
- Yang, J., Jamei, M., Heydari, A., Yeo, K. R., La Torre, R., De, F. M., Tucker, G. T., & Rostami-Hodjegan, A. (2006). Implications of mechanism-based inhibition of CYP2D6 for the pharmacokinetics and toxicity of MDMA. *Journal of Psychopharmacology*, 20, 842–849.
- Zhou, S., Zeng, S., & Shu, Y. (2021). Drug-drug interactions at organic cation transporter 1. *Frontiers in Pharmacology*, 12, 1–17.

SUPPORTING INFORMATION

Additional supporting information can be found online in the Supporting Information section at the end of this article.

How to cite this article: Alberto-Silva, A. S., Hemmer, S., Bock, H. A., da Silva, L. A., Scott, K. R., Kastner, N., Bhatt, M., Niello, M., Jäntschi, K., Kudlacek, O., Bossi, E., Stockner, T., Meyer, M. R., McCorvy, J. D., Brandt, S. D., Kavanagh, P., & Sitte, H. H. (2024). Bioisosteric analogs of MDMA: Improving the pharmacological profile? *Journal of Neurochemistry*, 00, 1–21. <https://doi.org/10.1111/jnc.16149>